A New Design Methodology for Hydraulic Cross-Flow Turbine and its Implementation

Goodarz Mehr[a,*], Mohammad Durali[b,**], Mohammad Hadi Khakrand[a], Hadi Hoghooghi[a]

[a] *Department of Mechanical Engineering, Sharif University of Technology, Tehran, Iran*
[b] *Professor of Mechanical Engineering, Sharif University of Technology, Azadi Avenue, Tehran 11155-9567, Iran*

arXiv:1702.07043v2 [physics.flu-dyn] 10 Apr 2017

Abstract

An extensive amount of research has been conducted on hydraulic Cross-Flow turbine over the past decades in order to improve its performance, but in several cases results are contradictory and little has been mentioned about the design process, so a universal, coherent methodology for designing a Cross-Flow turbine given the water head and volume flow rate seems most needed. In this article, we address this issue by introducing a design framework, both for the system-level and detail design phases. This methodology relies on theoretical expressions, numerical simulations, and experimental data, and is utilized to design a new Cross-Flow turbine and optimize its performance by investigating the effect of several parameters, such as admission angle, blade profile, and diameter ratio, on turbine's efficiency. The designed turbine seems to be able to achieve an efficiency of 82% that is maintained for water volume flow rates as low as 16% of the nominal value and water head variations up to 30%.

Keywords: Cross-Flow Turbine, Design, Development, Computational Fluid Dynamics (CFD), Optimization

1. Introduction

Hydropower has been utilized for more than a century and is the most common and most efficient source of renewable electricity generation [1]. In 2014, 4000 TWh of electricity was produced by hydropower and it accounted for 16.4% of world electricity, and 73.2% of total renewable electricity production. This amount is expected to increase to 4500 TWh by 2020 [2].

Generally, hydropower is produced by turbines installed behind large dams; however, the high initial cost of installation and power transmission, as well as the environmental challenges associated with dams, makes local power generation an attractive and efficient option, especially in rural, remote and mountainous areas [3–5]. Small turbines can be installed on rivers, fish farms, and water purification facilities to provide enough electricity for homes, farms and small plantations in remote areas [6]. However, the turbine used for this purpose should have unique characteristics, including an affordable price and easy and low maintenance cost. Also, a high efficiency under varying load conditions that is present in many local water sources is expected. These features are all present in a Cross-Flow turbine.

In a Cross-Flow turbine, water enters the rotor tangentially, passes through it transversely and exits from it radially, thereby transmitting the majority of its kinetic energy to the rotor. The specific speed of Cross-Flow turbines is greater than impulse Pelton turbines but lower than mixed-flow Francis turbines. A Cross-Flow turbine can achieve an efficiency of up to 86%, which is slightly less than other types of hydraulic turbines (Pelton, Francis, and Kaplan) [7]. It is suitable for applications where water head is between 2.5 and 200 meters and volume flow rate is between 0.025 and 13 cumecs [8]. A Cross-Flow turbine is generally used in micro and small power plants, with output powers ranging from 20 kW to approximately 5 MW [9]. Components of a typical Cross-Flow turbine are shown in Fig. 1.

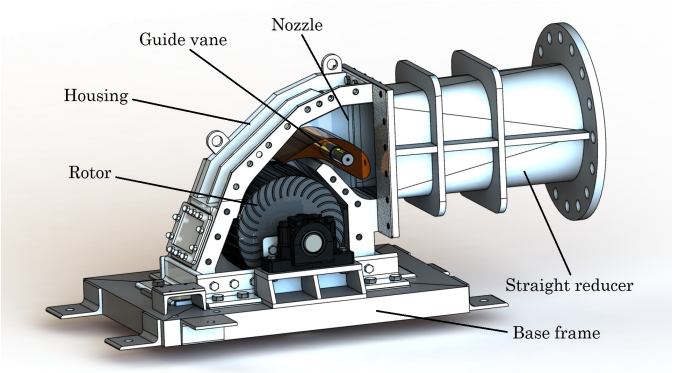

Figure 1: Components of a Cross-Flow turbine. The straight reducer is used to connect the circular discharge line to the rectangular entrance of the turbine. Some parts have been omitted to provide a better visual appearance.

In addition to having a simple structure and design, which results in a low manufacturing cost, the Cross-Flow turbine is particularly of interest because it has a flat efficiency curve [10]. When needed, the turbine can be built as a multi-cell turbine with a 1:2 division. This enables the turbine to handle low-flow conditions and operate at optimum efficiency for any water flow from 1/6 to full design flow rate. In addition, a Cross-Flow

*Corresponding author. Tel: +982188215833.
**Principal corresponding author. Tel: +982166165514.
Email addresses: goodarzm@alum.sharif.edu (Goodarz Mehr), durali@sharif.edu (Mohammad Durali), khakrand_mohammadhadi@mech.sharif.edu (Mohammad Hadi Khakrand), hoghooghihadi@alum.sharif.edu (Hadi Hoghooghi)

turbine does not require any special maintenance or treatment and is self-cleaning: water that passes through the turbine clears away any object in its path and prevents rotor clogging.

In the following two sections, we give a brief review of the theoretical equations proposed for designing the turbine, and previous studies. The ambiguous, inconsistent and sometimes contradictory nature of many of these results is discussed in order to demonstrate the need for a universal design framework.

2. Principles of operation and design

The two main parts of a Cross-Flow turbine are nozzle and rotor. The rotor is made up of two parallel discs that are joined to each other at the rim using several curved blades. The nozzle, which has a rectangular cross-sectional area, guides the water jet towards the rotor, which then strikes the blades on the rim, flows inside the channels between the blades for the first time, passes through the empty space in the middle of the rotor and flows through the mid-blade channels for a second time, exiting the rotor almost radially [11]. Nomenclature of the turbine geometry and water entering the first stage can be seen in Fig. 2.

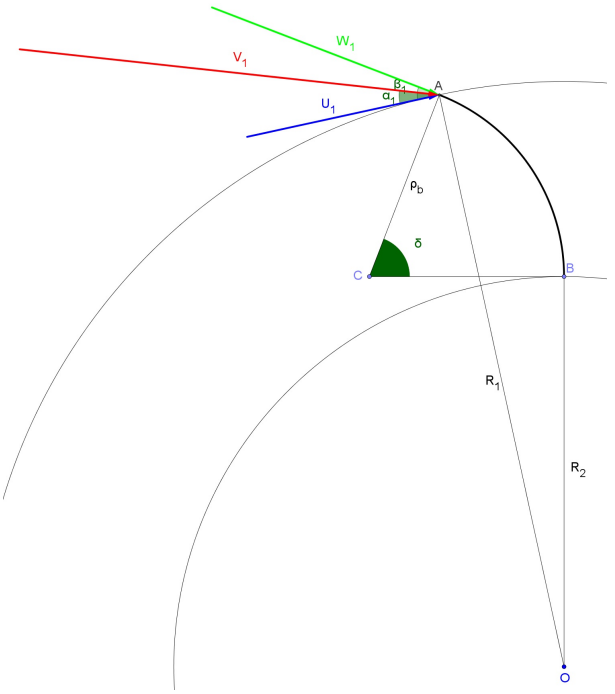

Figure 2: Nomenclature of the turbine geometry and water entering the first stage.

Using the Reynolds Transport Theorem, Mockmore and Merryfield showed that the highest value of efficiency that can be achieved theoretically is equal to

$$\eta_{t,\max} = \frac{1}{2} C_{l,n}^2 (1 + \psi) \cos^2(\alpha_1), \tag{1}$$

and it is achieved if

$$\frac{U_1}{V_1} = \frac{\cos(\alpha_1)}{2} \tag{2}$$

[11].

It is worth noting that η_t denotes turbine efficiency, which is the ratio of output power P_o to input power $P_i = \rho g Q H$, and should not be confused with turbine's hydraulic efficiency, which is defined as,

$$\eta_h = \frac{P_o}{P_i - P_e}. \tag{3}$$

P_e is the amount of water energy (total pressure) leaving the turbine. Hydraulic efficiency merely accounts for the amount of energy loss in the turbine, and ideally has a value of 1.

Using Eq. 2, the blade inlet angle is calculated using Eq. 4:

$$\tan(\beta_1) = 2 \tan(\alpha_1). \tag{4}$$

The blade exit angle β_2 is selected similarly, and its value must be equal to 90 degrees to avoid loss of efficiency [12].

The nozzle height can be determined using Eq. 5:

$$S_n = \sin(\alpha_1) R_1 \lambda. \tag{5}$$

Furthermore, Mockmore and Merryfield showed that, accounting for the centrifugal force of the rotor, the optimal rotor inner-to-outer diameter ratio (from here on called "diameter ratio") can be calculated using Eq. 6 [11]:

$$\left(\frac{D_2}{D_1}\right)^2 - \left[1 - \frac{1}{\cos^2(\beta_1)}\right]\left(\frac{D_2}{D_1}\right) - \tan^2(\beta_1) = 0, \tag{6}$$

and the rotor length by,

$$B = \frac{Q}{V_1 S_n} = \frac{Q}{V_1 \sin(\alpha_1) R_1 \lambda} = \frac{Q}{C_{l,n} \sqrt{2gH} \sin(\alpha_1) R_1 \lambda}. \tag{7}$$

To reduce manufacturing costs, turbine blades are assumed to be circular arcs having a constant thickness. The blade radius ρ_b is calculated using Eq. 8:

$$\rho_b = \frac{R_1^2 - R_2^2}{2(R_1 \cos(\beta_1) - R_2 \cos(\beta_2))}. \tag{8}$$

Similarly, for the blade central angle δ:

$$\delta = 2 \tan^{-1}\left(\frac{\cos(\beta_1) - \frac{R_2}{R_1}\cos(\beta_2)}{\sin(\beta_1) + \frac{R_2}{R_1}\sin(\beta_2)}\right). \tag{9}$$

3. Previous works

Australian engineer A. G. M. Michell, Hungarian inventor Donat Banki, and German entrepreneur Fritz Ossberger are generally credited as the first people to develop a Cross-Flow turbine. Michell patented his design in 1903, while Banki further developed it in West Germany, and the turbine became known as the Banki or Banki-Michell turbine. Banki suggested expressions for maximum turbine efficiency, diameter ratio and energy transfer at each stage and developed methods for designing rotor blades [13]. Meanwhile, Ossberger collaborated with Michell and improved his design, patenting the "Free-Jet

turbine" in 1922. After years of refinement, Ossberger obtained an Imperial Patent for the "Cross-Flow turbine" and started production in 1933 [14].

Mockmore and Merryfield laid the foundation of research on Cross-Flow turbine by translating Banki's transcripts into English. They also built an experimental model of this turbine and investigated the effect of rotational speed on turbine efficiency under various load conditions, verifying that the maximum efficiency occurred near the nominal speed calculated theoretically [11]. Since then, many researchers have performed experimental studies on Cross-Flow turbine. Khosrowpanah et al. tried to optimize the number of blades, diameter ratio, and admission angle [13]. Fiuzat et al. experimented on the turbine to determine the contribution of each stage to the output power [15]. Aziz et al. performed several experiments to identify the favorable values of angle of attack, diameter ratio, and the number of blades [16, 17]. Olgun conducted experiments to investigate the effect of diameter ratio and internal guide tubes in rotor on the performance of Cross-Flow turbine [18, 19]. Kaunda et al. performed several experimental and numerical studies to investigate the effect of water head, rotational speed and guide vane opening on the performance of Cross-Flow turbine [20, 21].

Since the early days of CFD, many researchers have used it solely or in conjunction with experiments to analyze and optimize Cross-Flow turbine performance. Choi et al. used CFD extensively to analyze the effect of various parameters, as well as nozzle shape, draft tube and air layer on the performance of Cross-Flow turbine [22–26]. De Andrade et al. investigated internal flow characteristics in a Cross-Flow turbine numerically [27]. Sammartano et al. used a transient model to analyze the behavior of a Cross-Flow turbine, investigate the effect of rotor shaft on turbine performance and optimize various parameters such as rotational speed, number of blades and diameter ratio. They further validated their results experimentally [10, 28–31]. Yassen used CFD to optimize various parameters, including number of blades, diameter ratio, angle of attack, admission angle, and blade and nozzle profiles [32], while Adhikari et al. studied the occurrence of cavitation using CFD [33].

Tab. 1 summarizes results of previous studies on the Cross-Flow turbine and contains values of turbine parameters used or optimized in each study. A - mark indicates the information has not been mentioned in the respective research. Also, "theo" represents a theoretical, "con" a conceptual, "num" a numerical, and "exp" an experimental study.

Table 1: Summary of turbine parameters used or optimized in previous studies. A - mark indicates a lack of information in that study.

Research details			Used or optimized parameters								
Researcher(s)	Research type	Research year	Water head (m)	Water volume flow rate (l/s)	Rotational speed (rpm)	Rotor diameter (mm)	Rotor length (mm)	Number of blades	Diameter ratio	Attack angle (deg)	Admission angle (deg)	Efficiency (%)
Mockmore and Merryfield [11]	exp	1949	2.7 - 5.5	62.9	270	333	305	20	0.66	16	-	68
Durali [12]	theo	1976	10	86.7	300	380	165	24	0.6	16	30	60
Durgin and Fey [34]	exp	1984	-	-	-	-	-	18	-	16	63	61
Fukutomi et al. [35]	theo/exp	1985	-	-	-	-	-	-	-	-	30 - 120	-
Khosrowpanah et al. [13]	exp	1988	0.335 - 2.60	20.4 - 44.2	87 - 356	304.8	152.4	15	0.68	16	90	80
Fiuzat et al. [15]	exp	1991	-	-	-	304.8	152.4	-	0.667	-	90	78.8
Aziz and Desai [16, 17]	exp	1991	0.340 - 0.343	25.6 - 25.8	-	304.8	152.4	25	0.68	24	90	84.49
Totapally and Aziz [36]	exp	1994	-	-	-	-	101.6, 152.4	35	0.68	22, 24	90	92
Joshi et al. [37]	exp	1995	2 - 9	-	-	300	325	24	0.66	16	36	64.8
Costa Pereira and Borges [7]	exp	1996	0.89 - 5.2	-	-	300	215	25	0.667	15	80	73.8
Reddy et al. [38]	exp	1996	3 - 9	90	360	300	325	24	0.66	16	36	67.58
Olgan [18]	exp	1998	4 - 30	14 - 55	400 - 1300	170	114	28	0.67	16	46	72
Olgan [19]	exp	2000	4 - 30	14 - 55	968 - 1107	170	114	24	0.54	16	46	70
Kaniecki [39]	exp/num	2002	10, 15	300, 195	410, 550	300	300, 150	30	0.667	16	-	79, 81
Kaniecki and Steller [40]	exp/num	2003	10, 15	300, 195	410, 550	300	296, 150	30	0.667	16	82, 105	74.3, 78
Choi et al. [22]	num	2008	2.9	-	-	250	150	26	-	-	120	65.7
Walseth [41]	exp	2009	-	-	350	270	-	24	0.696	16	120	77.5
Choi et al. [23]	exp/num	2010	20	516	530	-	500	30	-	-	-	-
De Andrade et al. [27]	exp/num	2011	35	135	1000	294	150	24	0.68	16	70	75
Haurissa et al. [42]	exp	2012	-	0.234	300	200	-	20	0.65	16	-	72.569
Choi and Son [24]	num	2012	46	176	1000	280	135	23	-	19	-	-
Kokubu et al. [25]	exp/num	2012	3.15	6.6, 44.4	280	250	17, 100	30	-	16	-	62.9
Kokubu et al. [43]	exp/num	2013	-	-	-	250	-	30	0.668	17	109	-
Sammartano et al. [10]	num	2013	14.2	60	757	161	93	35	0.646	22	90	85.6
Sammartano et al. [28]	exp/num	2014	-	60	750	161	93	35	0.646	22	90	82.1
Sammartano et al. [29]	con	2014	-	-	380	735	130	60	0.75	15	120	89
	con	2014	13.9	620	300	390	616	60	0.75	15	120	84
Sinagra et al. [30]	con	2014	32.7	620	360	385	530	50	0.65	15	120	89
Kaunda et al. [20]	exp	2014	3 - 10	-	350	268	-	24	0.693	16	90	79
Kaunda et al. [21]	num	2014	5	-	350	-	-	24	0.693	16	90	78
Reihani et al. [44]	num	2014	60	200	1000	300	152	19	-	16	-	63.73
Yassen [32]	num	2014	-	-	-	300	300	30	0.65	15	90	77.810
Sinagra et al. [31]	exp/num	2015	-	60	750	161	93	35	0.646	22	90	82.1
Chen and Choi [26]	exp/num	2015	20	465.0	530	340	500	30	-	-	120	81.3
Acharya et al. [45]	num	2015	10	100	642	200	-	22	-	-	-	80.76
Elbatran et al. [46]	con	2015	-	-	-	200	400	26	0.7	-	-	49
Elbatran et al. [47]	num	2015	-	-	-	200	380	26	0.684	16	-	52
Katayama et al. [48]	exp/num	2015	0.71	7	-	200	100	20	-	16	-	49.8
Costa Pereira and Borges [49]	theo/exp	2016	5.5	100	-	300	215	20	0.667	13	80	84.8
Adhikari et al. [33]	num	2016	3 - 10	56 - 105	200 - 700	316	150	20	0.68	16	69	69

Almost every study reviewed in Tab. 1 has investigated the performance of a low-head micro Cross-Flow turbine. Therefore, rotor diameter mostly has a value that falls between 150 and 350 millimeters. Moreover, Tab. 1 suggests that results obtained in these studies are partly inconsistent and even occasionally contradictory.

Most studies agree that an optimal angle of attack is between 12 and 20 degrees, with 16 being the favorable value. Only a few have concluded that an angle of attack greater than 20 degrees leads to a higher efficiency ([10, 28, 36]); however, it seems that in these studies the value of hydraulic efficiency is mistakenly reported in place of turbine efficiency, leading to the erroneous conclusion that 22 degrees is the optimal value for attack angle. Additionally, according to Tab. 1 the optimal value of diameter ratio is between 0.65 and 0.69.

Inconsistencies become notable when considering data on the number of blades and admission angle. While data in Tab. 1 suggests that the optimal value of admission angle is between 80 and 120 degrees, some researchers reported 90 degrees as the optimal value while others favored 120 degrees. Furthermore, it is seen that data in Tab. 1 for the number of blades is evenly distributed between 15 and 35 blades without any specific relation to site-specific values such as water head or volume flow rate. Therefore, no definite conclusion can be drawn on the optimal value of the number of blades based on Tab. 1.

Although these studies provide a good insight into the effect of each single parameter on the efficiency of the turbine, only a few of them provide a limited framework for designing a new turbine. None of these studies provide details about the system-level design, which includes defining product architecture and key parameters such as rotor diameter, while only a few (such as [10]) propose limited methodologies for the detail design phase.

A new design framework is proposed in this article that encompasses the system-level design as well as the detail design phases. This new methodology relies on theoretical expressions and experimental data for the system-level design phase and on CFD simulations for the detail design phase, which are validated by experimental data. To demonstrate its application, the proposed methodology is used to design and optimize the performance of a new Cross-Flow turbine, which not only achieves a high value of efficiency, but also maintains that efficiency under a wide range of load conditions.

4. Design methodology

Design and development of a new product normally comprises these five phases: concept development, system-level design, detail design, prototype testing and refinement, and production ramp-up [50]. To install a new hydraulic turbine, in the concept development phase it is essential to collect data on water head and volume flow rate of a potential site for several months (usually one year). This data should be analyzed to determine whether installation of a hydraulic turbine is technically feasible, and if so, what kind of turbine(s) should be used. Also, the project should be examined from a financial standpoint.

The next two phases, system-level design and detail design, explore determining the product architecture, parameter value selection, and geometry optimization [50].

4.1. System-level design

In the following sections, we establish a design framework for the system-level design phase, which primarily discusses the process of selecting key turbine parameters, and validate it using data from working turbines.

4.1.1. Design process

The first stage in the system-level design phase is defining product architecture and identifying its components. Cross-Flow turbine typically consists of a nozzle from which water is discharged to a rotor. This simple design has evolved over the years and has taken various forms. The architecture that we use consists of four major components: nozzle, rotor, housing and guide vane, as seen in Fig. 3. The rotor should be installed inside the housing at the nozzle exit within a small clearance which ensures that efficiency losses due to air entrainment are kept at a minimum. Also, a curved guide vane should be used inside the nozzle to guide and regulate water flow. Moreover, a low-head turbine can feature a draft tube to increase the net water head and an air vent to regulate the pressure inside the housing.

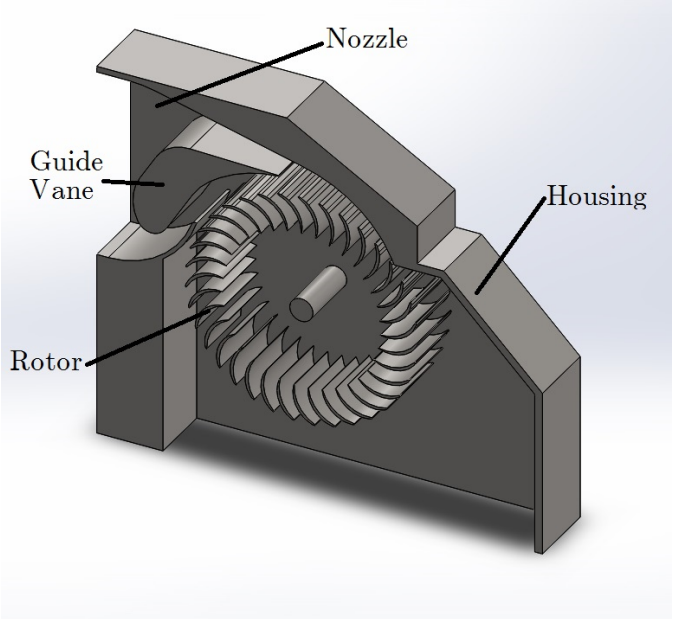

Figure 3: Cross-section of a Cross-Flow turbine. Water that enters the nozzle is directed by the guide vane to enter the rotor with the proper angle.

The second stage is determining turbine parameter values, including rotor diameter and length, diameter ratio, rotational speed, angle of attack, blade inlet and exit angles, admission angle, and the number of blades. Note that values assigned to some of these parameters are preliminary and subject to change in the detail design phase.

In order to facilitate the process, we utilize the theoretical relations presented in sec. 2 to determine parameter dependency. Specifically, if values of rotor diameter, angle of attack, admission and blade exit angle, and the number of blades - which we call key turbine parameters - are known, rotor length is obtained from Eq. 7 and rotational speed is calculated using Eq. 2. Furthermore, blade inlet angle is computed from Eq. 4 and diameter ratio is obtained from Eq. 6. Finally, nozzle height and blade specifications are determined using Eq. 5, Eq. 8 and Eq. 9, respectively. Therefore, it suffices to determine the value of key turbine parameters, and other parameters will be determined accordingly.

As discussed in sec. 2, the value of blade exit angle must be 90 degrees to avoid loss of efficiency. Based on the discussion in sec. 3 we use the universally accepted value of 16 degrees for angle of attack, as well as preliminary values of 120 degrees for admission angle and 32 for the number of blades, although they will be optimized in the detail design phase.

We utilize a parameter similar to the specific speed to determine the value of rotor diameter. This parameter has been computed for numerous hydraulic turbines (including Cross-Flow turbine) experimentally and is used to determine the optimal range of rotational speed of a turbine based on water head and volume flow rate [51]. For a Cross-Flow turbine, this information leads to the value of rotor diameter by using Eq. 2.

Eq. 10 presents the dimensionless specific speed of turbomachinery. This definition is rarely used and the definition given in Eq. 11 that uses Metric units is more common [52].

$$N'_s = \frac{\omega \sqrt{\frac{P_o}{\rho}}}{(gH)^{\frac{5}{4}}}, \tag{10}$$

$$N'_{sd} = \frac{N(\text{rpm})\sqrt{P_o(\text{kW})}}{[H(\text{m})]^{\frac{5}{4}}}. \tag{11}$$

By slightly changing the definition of N'_{sd}, a new parameter is obtained which is denoted by N_q, and is defined as,

$$N_q = \frac{N(\text{rpm})\sqrt{Q(\text{cumecs})}}{[H(\text{m})]^{\frac{3}{4}}}. \tag{12}$$

The main advantage of N_q over the traditional N'_{sd} is that instead of using the output power to calculate the parameter, which is usually unknown during the system-level design phase, only site-specific values of Q and H are used.

The value of N_q has been calculated for various types of turbines experimentally, and the results are plotted against water head to obtain recommended regions of optimal performance for different types of turbines [51]. This diagram is shown in Fig. 4. It is observed from Fig. 4 that the value of N_q for a Cross-Flow turbine is slightly greater than its value for a Pelton turbine, but almost the same as that of a Francis turbine. The main difference between these turbines is in the operating range of water head; Cross-Flow turbines are mostly used for low-head applications, whereas Francis and Pelton turbines are used in medium- and high-head sites, respectively.

The process described here for the system-level design phase can be summarized in the flowchart in Fig. 5. As explained earlier, this process receives water head and volume flow rate values as inputs and leads to preliminary values of key turbine parameters, as well as turbine's architecture.

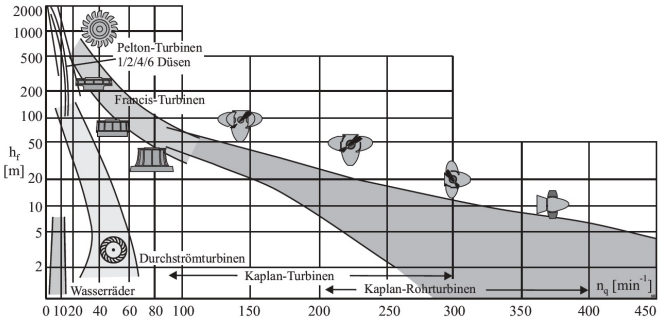

Figure 4: Optimal range of N_q for different types of hydro turbines [51]. Durchstromturbinen means Cross-Flow turbine and Wasserrader means Water wheel. Other names are self-explanatory.

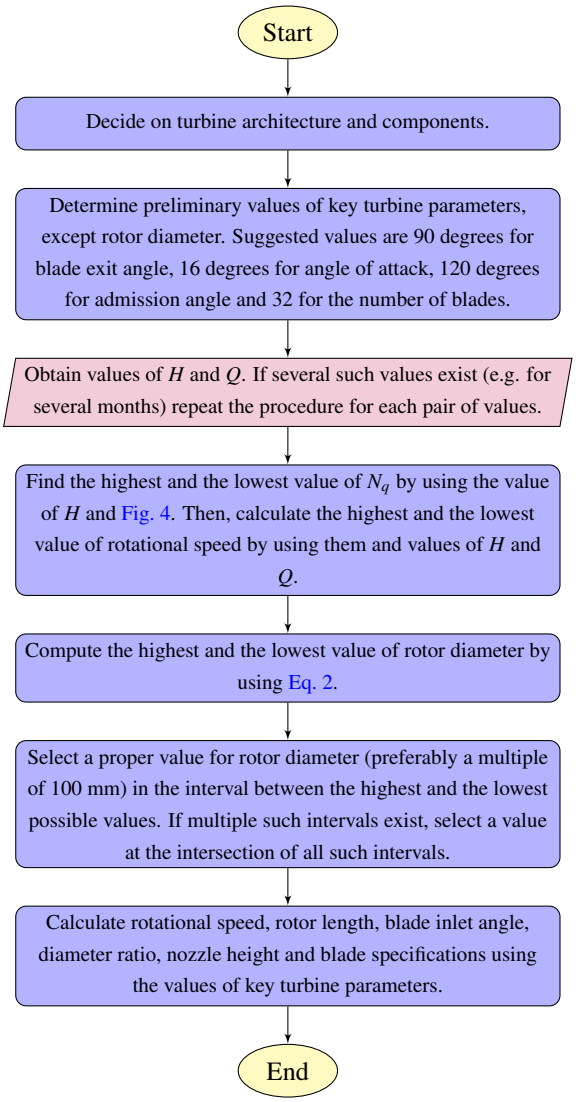
Start
Decide on turbine architecture and components.
Determine preliminary values of key turbine parameters, except rotor diameter. Suggested values are 90 degrees for blade exit angle, 16 degrees for angle of attack, 120 degrees for admission angle and 32 for the number of blades.
Obtain values of H and Q. If several such values exist (e.g. for several months) repeat the procedure for each pair of values.
Find the highest and the lowest value of N_q by using the value of H and Fig. 4. Then, calculate the highest and the lowest value of rotational speed by using them and values of H and Q.
Compute the highest and the lowest value of rotor diameter by using Eq. 2.
Select a proper value for rotor diameter (preferably a multiple of 100 mm) in the interval between the highest and the lowest possible values. If multiple such intervals exist, select a value at the intersection of all such intervals.
Calculate rotational speed, rotor length, blade inlet angle, diameter ratio, nozzle height and blade specifications using the values of key turbine parameters.
End

Figure 5: Flowchart of the design process for the system-level design phase. This process leads to preliminary values of key turbine parameters and turbine's architecture.

4.1.2. Methodology validation

In this phase, use of previous results to determine the values of key turbine parameters - except for rotor diameter - guarantees that they are in the optimal range. The recommended region in Fig. 4 is based on experimental data, but to ensure that the information is current and accurate, we check that region against publicly available data from several OSSBERGER^{TM} turbines, which is tabulated in Tab. 2.

Table 2: Performance specifications of OSSBERGER^{TM} Cross-Flow turbines. These values are gathered mostly from excerpts of magazines published on the OSSBERGER^{TM} website. A - mark indicates a lack of information.

Site	Water head (m)	Water volume flow rate (cumecs)	Rotational speed (rpm)	Output power (kW)	Efficiency	Rotor diameter (mm)
Puente Alto [53]	34.2	7.12	177	2000	84.0	-
Allipen [54]	20	9	139	1480	84.1	-
Schluchsee [55, 56]	37.6	4.68	214.3	1442	83.8	1000
Sloat [56]	114	0.052	1200	45.3	78.2	-
Great Dhunn Dam [57]	35 - 45	0.4	610	140	-	-
Leerstetten [58, 59]	24.67	6	180	1186	81.9	1000
Vordernberger Bach [59, 60]	15	2.8	228.3	346	84.3	-
Schonebach [61]	18.75	2.7	202	414	83.6	-
Cyimbili [14, 62]	164.78	0.22	1000	302	85.2	-
Goodyear Lake 1 [63]	10	8.5	135	650	78.2	1000
Goodyear Lake 2 [63]	10	11.5	104	850	75.6	1250
Zahlen (Haptmaschine) [64, 65]	7.1	4.5	127	263	84.2	800
Zahlen (Wehrmaschine) [64, 65]	5.4	1	217	43.4	82.2	400
Oberwolz [66]	58	1.9	375	940	87.2	-
Hitzinger [67]	78	0.6	750	390	85.2	-
Engstligenalp [68]	56.9	1.35	500	623	82.9	-
Geistermuhle [69]	5.7	0.16	320	7.1	79.6	-
Kaltenegger [70]	66	0.8	600	-	-	-

In order to validate the proposed methodology, the value of N_q for each turbine is calculated using data from Tab. 2. Then, these values are plotted against the optimal region proposed in Fig. 4. The result is presented in Fig. 6.

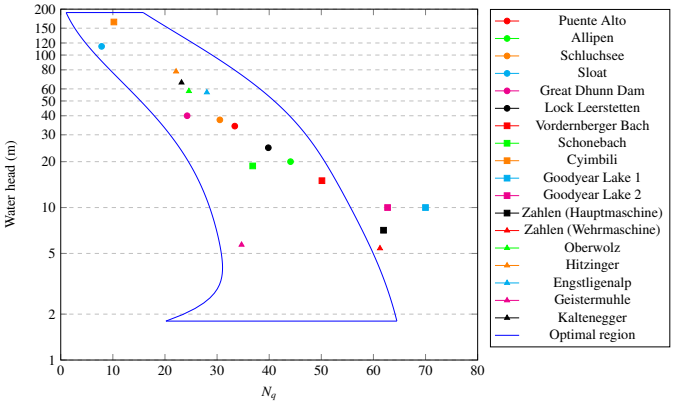

Figure 6: Plot of water head versus N_q for OSSBERGER^{TM} turbines. The value of N_q for most of the OSSBERGER^{TM} turbines is located inside the recommended region.

From a total of 18 turbines, 14 fall inside the designated region in Fig. 6. The four remaining turbines are those installed at Goodyear Lake and Zahlen power plants. Turbines of the Goodyear Lake power plant were installed during the 1970s and have an efficiency of approximately 75% which is far less than the optimal value of 85% [63], so it is natural for them to be located outside of the optimal region. Furthermore, note that all of these four turbines have very low rotational speeds (which is the only non-site-specific variable affecting the value of N_q), and lowering that speed any further may require a bigger gearbox or a more expensive generator which may impact the overall efficiency and cost of the power plant. This can explain why a higher rotational speed is preferred instead.

Overall, the conclusion that can be drawn from the above argument is that unless there are concerns about the impact of other components of the system on the overall efficiency of the power plant, the value of N_q for a Cross-Flow turbine should be in the designated region in Fig. 4 for the turbine to operate at optimal conditions.

4.2. Detail design

The detail design phase encompasses a broad range of activities and much of it is beyond the scope of this article. Our focus is on the first level of this phase for a Cross-Flow turbine, which is specifying its interior geometry.

4.2.1. Design process

This level can be broken down into three steps. The first step is nozzle design for nominal operating conditions; the second step is optimizing turbine parameter values for nominal operating conditions; and the final step is analyzing turbine's performance under various load conditions and making necessary modifications in order to achieve a constant value of efficiency for a wide range of water head and volume flow rate. This approach is further illustrated in Fig. 7.

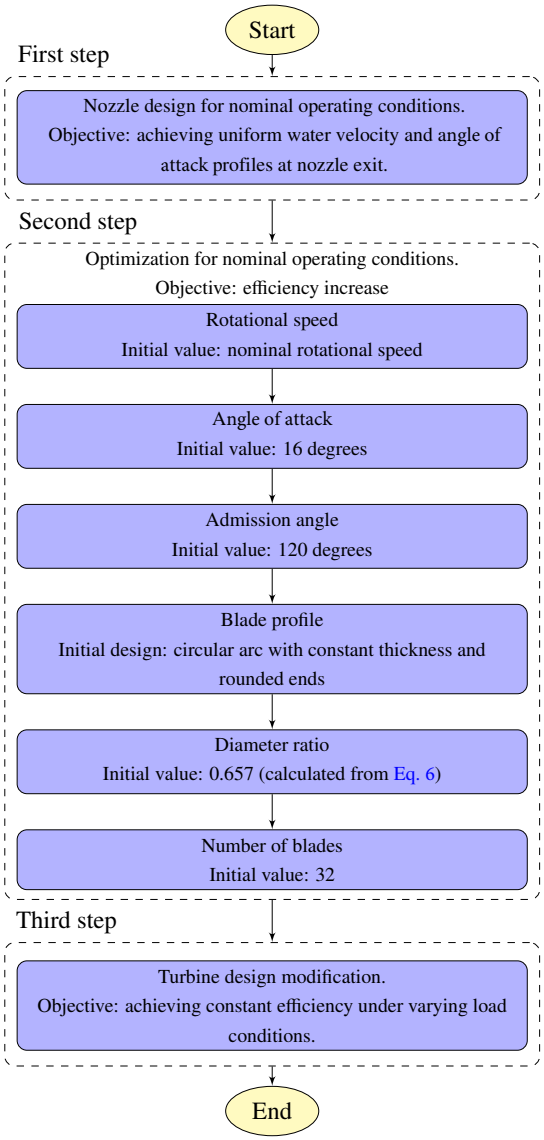
Start
First step
Nozzle design for nominal operating conditions.
Objective: achieving uniform water velocity and angle of attack profiles at nozzle exit.
Second step
Optimization for nominal operating conditions.
Objective: efficiency increase
Rotational speed
Initial value: nominal rotational speed
Angle of attack
Initial value: 16 degrees
Admission angle
Initial value: 120 degrees
Blade profile
Initial design: circular arc with constant thickness and rounded ends
Diameter ratio
Initial value: 0.657 (calculated from Eq. 6)
Number of blades
Initial value: 32
Third step
Turbine design modification.
Objective: achieving constant efficiency under varying load conditions.
End

Figure 7: Flowchart of the design process for the detail design phase.

Fig. 7 reveals that in the second step, each parameter is optimized separately instead of optimizing them all at once. The reason is that if the latter approach was adopted with a numerical algorithm to optimize all of the parameters (like the Genetic Algorithm) the effect of each parameter on turbine's performance could not be understood. Alternatively, if an experimental method was implemented, and assuming that at least three values were considered for each parameter, at least $3^6 = 729$ experimental setups would be required which is both economically unjustifiable and time-consuming. Fig. 7 also shows that nozzle design and parameter value optimization are done separately because it helps reduce the time needed for each of these steps.

Initially, this methodology is highly iterative and several cases must be analyzed; however, the results are scalable. Once the geometry has been determined, it can be scaled with respect to rotor diameter to obtain the geometry of a larger or smaller turbine. This is true for many other parameters as well. Exceptions to this rule are diameter ratio and number of blades, which are dependent to each other by a parameter called solidity [12], and their values slightly depend on water head. Therefore, they should be optimized on a case by case basis.

This methodology, which many researchers have partially used in their studies, can be implemented both experimentally and numerically. A numerical approach is preferred, since an experimental setup is both prolonged and expensive. Nevertheless, in a numerical approach it is essential to use a correct CFD model and to verify and validate that model using experimental data.

4.2.2. CFD model

In this research, we used SolidWorks® to design CAD models, ANSYS® Meshing to mesh the geometry and ANSYS® CFX to perform CFD simulations. However, any other native or commercially available CAD or CAE program may be used, as long as the CFD model is validated by experimental results.

The first step of performing a numerical simulation is designing the geometry. The focus of this step is on the interior design of the turbine, so it suffices to prepare a simple model of turbine's interior. Moreover, it is a good practice to use a parametric design for easy geometry scaling. Since CFX does not allow two-dimensional CFD simulations, a cross-sectional slab with a small width is prepared and used instead, with symmetry boundary condition assigned to the sides [10].

Next, the geometry must be meshed, which is highly important since mesh size and quality directly impacts solution time and the accuracy of results. For a two-phase CFD analysis unstructured mesh is favored over structured meshing since the fluid flow - especially that of air - is largely undetermined. The majority of the meshing consists of tetrahedral elements, each having a size that is equal to the width of the slab [10]. However, near-wall regions have been meshed using Meshing's built-in pre-meshing inflation algorithm with multiple (more than 20) layers of prismatic elements [10, 21]. The first layer has a height of only 10 micrometers and layer heights grow geometrically by a factor of 1.05. This resolution is necessary for error reduction when using the Shear Stress Transport (SST) turbulence model [71, 72]. A sample meshing is shown in Fig. 8.

After geometry meshing is complete, a CFD model should be defined to simulate fluid flow. In our models we assume that the flow condition is steady and that buoyancy forces are negligible due to the small elevation difference in the turbine in comparison to the water head. Furthermore, since no noticeable temperature change occurs during turbine's operation, we assume that heat transfer between the turbine and its surroundings is negligible as well.

We used the Shear Stress Transport (SST) turbulence model with automatic wall function to model the flow [72]. The SST model gives highly accurate predictions of the onset and the amount of flow separation under adverse pressure gradients [71, 73], which is extremely useful when studying the effect of blade profile on turbine efficiency.

For the first step, a single-phase model with water as the

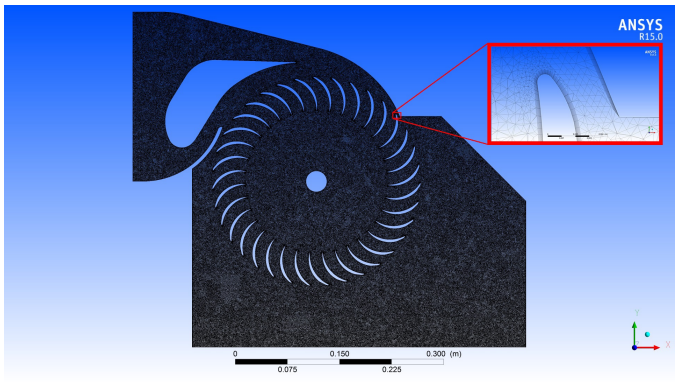

Figure 8: Turbine CFD meshing. Near-wall regions have been resolved into several layers of prismatic elements, while the rest of the turbine is meshed mostly with tetrahedral elements.

only phase is used to simulate flow in the nozzle, and the convergence target is set to 1.0e-08 to obtain accurate results.

As stated before, symmetry boundary condition is assigned to the sides, and static pressure at the outlet is set to 1 atm. Mass flow rate boundary condition is assigned to the inlet because it gives the most robust configuration and is not sensitive to initial conditions. The inlet total pressure is an implicit result of the simulation [71]. A smooth no-slip wall boundary condition is assigned to the rest of the surfaces, and initial conditions are determined automatically by the software. These boundary conditions are illustrated in Fig. 9.

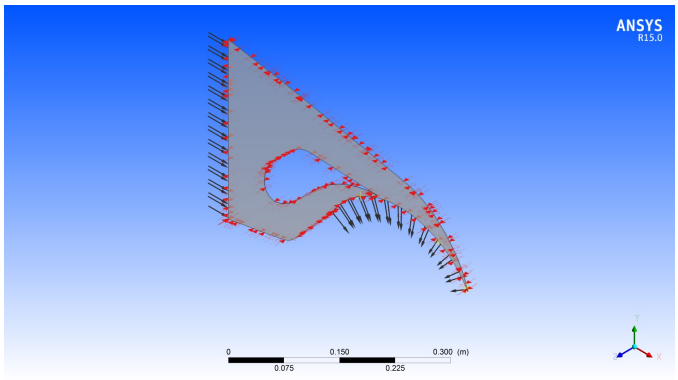

Figure 9: Nozzle boundary conditions: mass flow rate at the inlet, static pressure at the outlet, and symmetry at the sides. The arrows indicating inlet and outlet boundary conditions are figurative, as the flow through the outlet surface is not in the radial direction.

The CFD model used for the second step is more complex because it models the rotation of the rotor, and is very similar to the model used by Kaunda et al. [21]. In this model, the rotor is divided into two separate domains, one is rotating and consists of the area surrounding the blades, while the other is stationary and comprises both the inside of the rotor as well as the outside space in the housing.

We used a multiphase model utilizing both water and air as continuous fluids for the stationary domain. Additionally, since a well-defined interface exists between water and air, we utilized a homogeneous turbulence model [21]. Surface tension between the two phases is also modeled with air as the primary fluid. The model used for the rotary domain is the same, except that the domain revolves around the rotor's axis.

To obtain accurate results, a physical timescale equal to $\frac{0.1}{\omega}$ is used, where ω is in rad/s [72], and the convergence target is set to 1.0e-06. Additionally, we utilized advanced options like Rhie-Chow pressure-velocity coupling to achieve a smooth pressure field [73].

In the second step, it is assumed that water enters the rotor with the desired velocity and angle so that we can analyze the effect of selected parameters on the turbine's performance. Therefore, components of water velocity in cylindrical coordinates are defined at the rotor inlet, water's volume fraction is set to 1, and that of air is set to 0. At the outlet, an opening boundary condition is used with the static pressure set to 1 atm, and values of volume fraction and turbulence are assumed to have a zero gradient. Same as before, symmetry boundary condition is assigned to the sides, while a smooth no-slip wall boundary condition is given to the housing and rotor blades. A rotating wall boundary condition is also assigned to the rotor shaft, having the same speed as the rotor [21]. These boundary conditions are illustrated in Fig. 10.

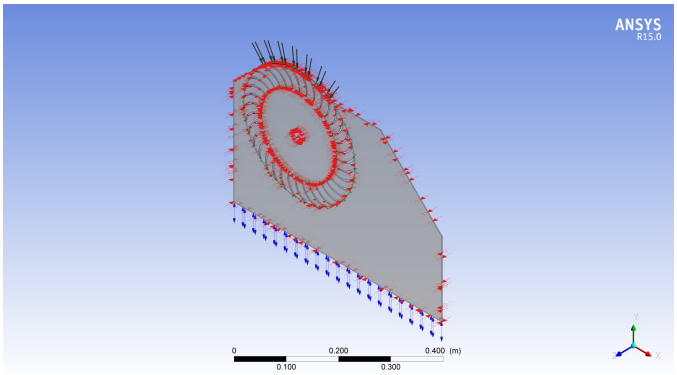

Figure 10: Rotor boundary conditions: water velocity components at the inlet, opening at the outlet with a constant static pressure, and symmetry at the sides.

The frozen rotor frame change model is utilized to model the interface between the stationary and rotating domains. This model treats the flow from one domain to the next by changing the frame of reference while maintaining the relative position of the components. It has the advantages of being robust, using fewer computer resources than other frame change models, and being well suited for high blade counts. However, using this model may result in inadequate prediction of physics for local flow values, and the results are slightly sensitive to the relative position of the stationary and rotating domains [72].

The CFD model used for the third step is the same as the previous step, except that now the body is divided into three domains: one stationary domain for the nozzle, one rotating domain for the rotor, and another stationary domain for the housing. The boundary conditions and interfaces are the same as well, except at the nozzle inlet. In order to obtain accurate results, first a simulation is performed using the mass flow rate boundary condition, then the boundary condition is changed to total pressure and the previous result is used as the initial con-

dition of the new simulation. These boundary conditions are illustrated in Fig. 11.

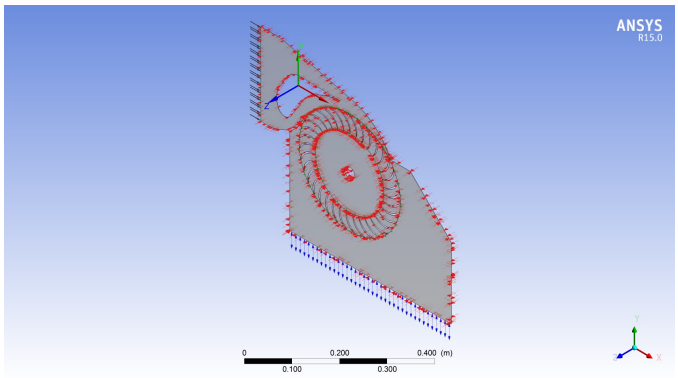

Figure 11: Turbine boundary conditions. They are the same as the previous step except at the nozzle inlet, which is mass flow rate at first and is changed to total pressure during the simulation.

4.2.3. CFD model validation

Several methods have been suggested for validation of a CFD model, including iterative convergence examination, consistency examination, spacial (grid) convergence examination, temporal convergence examination and model uncertainty examination. However, the best method is still the comparison of CFD results to experimental data, because experimental data is the observation of the "real world" in some controlled manner. [74, 75].

In order to validate the proposed CFD model, we used it to simulate the operation of a prototype Cross-Flow turbine designed and developed by Durali System Design and Automation (DSDA), which was tested under various load conditions experimentally to examine its efficiency. In the end, simulation results are compared to experimental data to check their agreement and model validity.

Experimental setup. Experimental tests were carried out at the testing facility of Water Research Institute of Iran (WRI) located in Tehran which is 1300 meters above the sea level. The facility consists of a water pumping system and a test stand on which the prototype Cross-Flow turbine is coupled to a synchronous generator. The experimental setup is similar to the one used by Sammartano et al. [28].

The experimental setup operates in a closed loop mode and is composed of an open tank reservoir, a suction pipe, four centrifugal pumps (to simulate various flow conditions) and a discharge pipe that is connected to the test stand. The rotor shaft is coupled to the generator shaft using pulleys and V-belts, and the electrical characteristics of the generated power are measured using a power analyzer unit. The generator has four poles and a speed of 1500 rpm when used with 50 Hz electricity. Several other instruments are used to measure different variables, and a summary of their specifications is available in Tab. 3.

Measurements are made according to the IEC41 standard for hydraulic turbine testing. Also, each test case is performed

Table 3: Specifications of measurement instruments used for testing the prototype Cross-Flow turbine developed by DSDA.

Measurement instrument	Uncertainty amount	Measured value	Full-Scale Output (FSO)
pressure transducer	0.5% FSO	inlet pressure	10 bar
flow meter	0.2% FSO	discharge flow	2222.2 l/s
power analyzer	1.0%	generator output	9.999 MVA
tachometer	0.1%	turbine speed	100000 rpm

5 times, and the average value of the results is reported as the final value.

Turbine efficiency is calculated using Eq. 13,

$$\eta_t = \frac{VI}{\eta_g \eta_m \rho g Q H}. \tag{13}$$

Values of V and I are read from the power analyzer, the value of Q is determined by the flow meter, and the value of H is indicated by the pressure transducer.

The generator has an average efficiency of 91.3% during the experiments which, after multiplication by an altitude factor of 0.982, reduces to 89.7%. The mechanical transmission system has an overall efficiency of 94.1% (accounting for the belts, pulleys, and bearings), which brings the overall transmission efficiency ($\eta_g \times \eta_m$) down to 84.4%.

The uncertainty of η_t is determined by the Root of the Sum of the Squares (RSS) rule for uncertainty propagation using individual uncertainties of the variables involved [76]. Specifically, the uncertainty associated with η_t is given by Eq. 14,

$$\frac{\Delta\eta_t}{\eta_t} = \Big[(\frac{\Delta V}{V})^2 + (\frac{\Delta I}{I})^2 + (\frac{\Delta\eta_g}{\eta_g})^2 + (\frac{\Delta\eta_m}{\eta_m})^2 + (\frac{\Delta Q}{Q})^2 + (\frac{\Delta H}{H})^2\Big]^{\frac{1}{2}}. \tag{14}$$

According to Tab. 3, the uncertainty of generated power is 1.0%, the uncertainty in the value of water volume flow rate is 4.44 l/s, and that of water head is 51.1 cm. Also, the uncertainty of generator efficiency is 0.5% and that of mechanical transmission system efficiency is 2%.

Results. The prototype turbine was designed for a nominal water head of 45 meters and volume flow rate of 100 l/s, with a rotational speed of 1074 rpm. Numerical simulations were performed in five different operating conditions using the proposed CFD model, and the turbine was tested under those same conditions to evaluate its efficiency. The operating conditions, numerical and experimental efficiencies and uncertainty values are tabulated in Tab. 4 and shown in Fig. 12.

As can be seen from Fig. 12, there is a satisfactory agreement between the experimental and numerical results, and the value of absolute error does not exceed 1.5% which validates the proposed CFD model (compare for example to the results of Kaunda et al. [21] or Sammartano et al. [28] who consider a value of 5% absolute error acceptable). It is worth noting that the relatively large value of uncertainty in experimental results is caused by two factors: first, turbine efficiency variation due

Table 4: Operating conditions and the results of CFD simulations and experimental tests performed on the prototype turbine to validate the CFD model.

Case number	Water head (m)	Water volume flow rate (l/s)	CFD efficiency (%)	Experimental efficiency (%)	Experimental uncertainty (%)	Relative error (%)
1	25.2	85.1	32.1	33.4	6.1	3.9
2	35.0	95.2	49.9	49.9	5.4	0
3	35.1	113.3	52.6	53.7	4.8	2.0
4	45.2	119.7	59.7	58.2	4.5	2.6
5	45.3	132.7	60.6	59.2	4.2	2.4

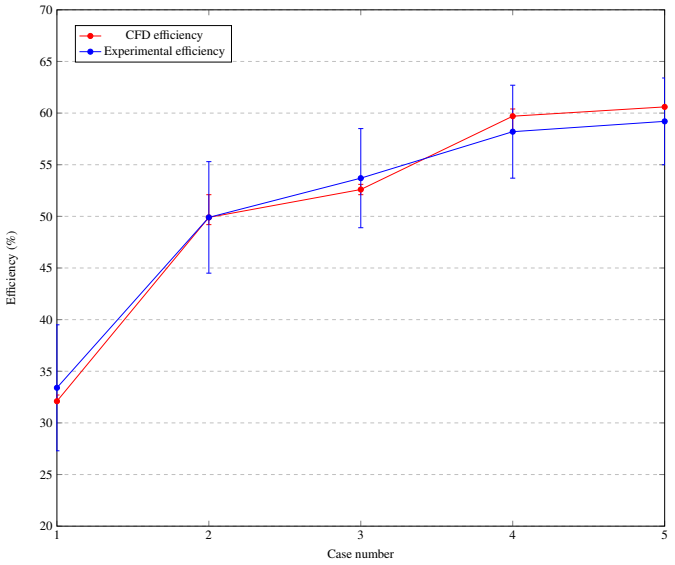

Figure 12: A comparison between the efficiencies obtained from CFD simulations and experimental tests performed on the prototype turbine. The results are in good agreement, validating the proposed CFD model.

to the changing relative position of the rotor and the nozzle and second, the large relative uncertainty of the flow meter.

Fig. 13 shows the operating prototype turbine, and Fig. 14 shows the distribution of total pressure inside the turbine that was obtained from the simulation results. It is evident from Fig. 14 that water flow follows the correct path inside the turbine; however, water exits the turbine in a different manner than the way observed in Fig. 13. This discrepancy is the result of using the frozen rotor frame change model, because when moving from a stationary domain into a rotating domain, the frozen rotor model only changes the frame of reference and not the relative position of the two domains.

Fig. 15 gives a closer look at velocity vectors entering the rotor and shows that the main cause of power loss is the flow separation that occurs at the tip of several blades which prevents water from transferring its energy to the rotor. Also, a portion of the water in the front and back of the turbine scarcely enters the rotor because of its centrifugal tendency, which results in the loss of power.

5. Methodology implementation

The final step is to validate the methodology and show that it can be successfully used to design a high-efficiency Cross-Flow turbine. To that end, we used the new methodology to design a turbine with a much higher efficiency which will replace the prototype turbine developed by DSDA. We designed the turbine for a nominal water head of 10 m and volume flow rate of 200 l/s. This nominal operating condition is one of the most prevalent hydro potentials in Iran.

Figure 13: The prototype turbine in operation.

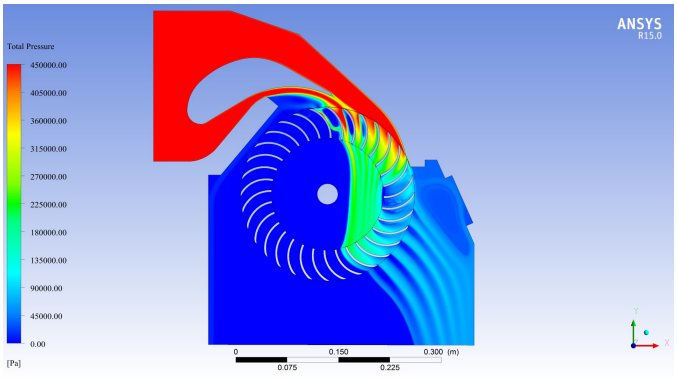

Figure 14: Distribution of the total pressure inside the turbine for one of the CFD simulations. The water follows the right path inside the turbine but exits it in a different manner than what observed during the experiments, which is a result of using the Frozen Rotor frame change model.

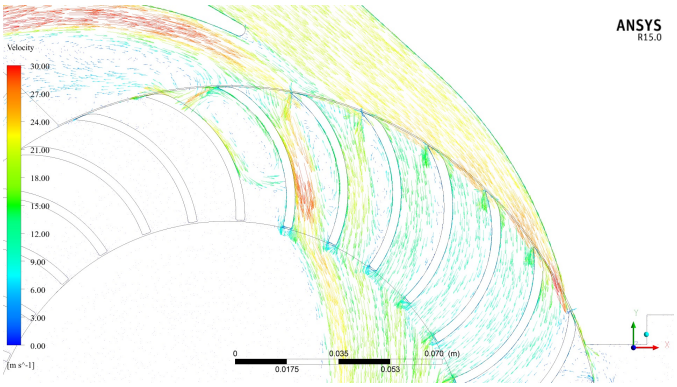

Figure 15: Velocity vectors entering the rotor. Inappropriate design of rotor blades causes velocity vectors that enter the rotor to deflect and results in flow separation, which ultimately results in the loss of efficiency.

5.1. System-level design

Preliminary values of key turbine parameters, except rotor diameter, are selected according to the process described in Fig. 5. To select the value of rotor diameter by using Fig. 4, for a 10 m water head the minimum and the maximum possible values of N_q are 28 and 56, respectively, hence by using Eq. 12, the minimum and the maximum possible values of rotational speed are obtained to be 352 and 704 rpm, respectively. Therefore, by using Eq. 2 the maximum and the minimum possible values of rotor diameter are calculated as 365 and 183 mm, respectively.

According to Fig. 5, two possible values for rotor diameter are 300 and 200 mm; however, the 300 mm diameter rotor is preferred because it results in less centrifugal force (which causes efficiency loss) and reduces the possibility of cavitation [33]. Nevertheless, this choice implies the use of a transmission system with a higher step up ratio which may impact overall efficiency.

After the value of rotor diameter is determined, equations that were introduced in sec. 2 are utilized to calculate the values of the remaining turbine parameters. These values are shown in Tab. 5. Note that the aspect ratio (the rotor diameter to length ratio) is $\frac{20}{11}$, which results in a higher efficiency compared to rotors with an aspect ratio of approximately 1 [13].

Table 5: Preliminary values of turbine parameters for the new turbine.

Turbine parameter	Value
rotor diameter (mm)	300
rotational speed (rpm)	429
rotor length (mm)	165
blade inlet angle (deg)	30
nozzle height (mm)	86.5
blade radius (mm)	49.1
blade central angle (deg)	73.8

5.2. Detail design

In this phase, using the values that were determined in the system-level design phase, the geometry of the turbine is designed and optimized. As discussed in sec. 4, this is done in three steps: the nozzle and the rotor are designed and optimized for the nominal operating conditions separately, then the whole turbine is tested under different load conditions and modified as necessary so that it can maintain a high efficiency over a wide range of operating conditions.

5.2.1. First step

The objective of this step is to design a nozzle that has an approximately uniform water velocity and angle of attack profile at its exit to ensure the optimal entrance of the water jet to the rotor. In the beginning, we prepared a preliminary sketch of the nozzle and guide vane based on the following criteria:

- the guide vane must be able to close the water passage completely by rotating around its axis;
- the sum of the heights of the passages below and above the guide vane should equal to the value obtained for nozzle height (in this case 86.5 mm); and
- nozzle ends on both sides of the admission arc must form an angle equal to the angle of attack with the tangent to the arc at those points (in this case 16 degrees).

Next, we used an iterative approach to optimize the nozzle geometry. Starting from the initial geometry, water flow through the nozzle is simulated and velocity and angle of attack profiles at the nozzle exit are plotted. Then these profiles are used to alter the geometry, through which water flow is simulated again. This iterative process is carried out until satisfactory profiles are achieved. For the present case, the initial and final nozzle geometries are shown in Fig. 16; Fig. 17 illustrates the velocity profiles and Fig. 18 the attack angle profiles of those nozzles.

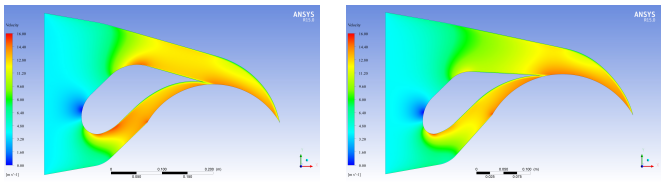

(a) initial nozzle (b) final nozzle

Figure 16: Water velocity distribution inside the nozzle. Note that velocity changes in the final nozzle are less abrupt compared to the initial nozzle.

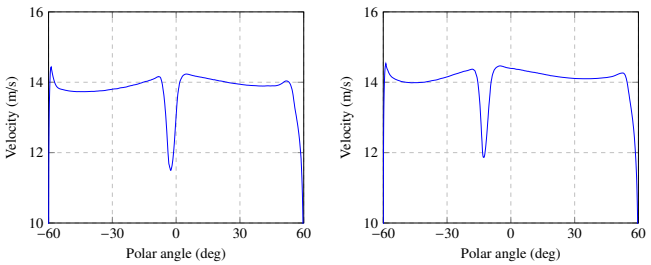

(a) initial nozzle (b) final nozzle

Figure 17: Velocity profiles at the nozzle exit. The notch at the middle of the profile corresponds to the tip of the guide vane.

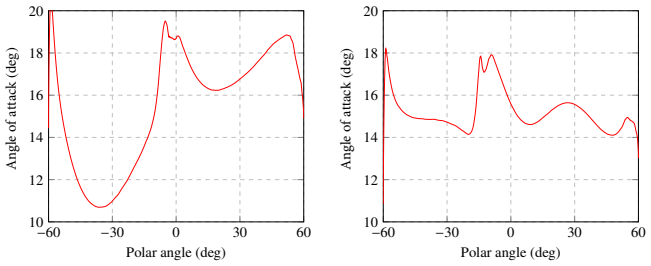

(a) initial nozzle (b) final nozzle

Figure 18: Angle of attack profiles at the nozzle exit. The profile for the final nozzle is more uniform compared to the initial nozzle.

Fig. 17 illustrates that both nozzles have approximately uniform velocity profiles because the value of velocity vectors at the exit depends only on nozzle height. However, Fig. 18 reveals a considerable difference in the attack angle profiles. The

reason for this difference is that attack angle is much more dependent on the nozzle geometry than velocity, and several parts of the nozzle geometry play a crucial role in determining it. In the final nozzle, the curve below the guide vane and the curve at the end of the nozzle are linear in terms of polar angle (which is explained in detail by Sammartano et al. [10]).

As can be seen from Fig. 16, the final nozzle has smoother curves, which prevents an abrupt increase in water velocity and reduces flow separation at the bends above and below the guide vane. Furthermore, Fig. 17 shows a notch at the middle of the profile. This notch is located at the tip of the guide vane and has a lower velocity than other regions because of the fully developed boundary layers on both sides of the guide vane that merge at that point.

Calculations show that the values of nozzle loss coefficient for the initial and final nozzles are 0.972 and 0.977, respectively. Using the latter value and Eq. 1, and assuming that the value of rotor loss coefficient is equal to 0.94, the maximum possible efficiency for this design is 85.6%.

5.2.2. *Second step*

The objective of this step is to optimize the value of the most important turbine parameters to increase the efficiency of the turbine and evaluate the individual effect of each parameter on it. Initial values of the parameters are set equal to the values obtained in subsec. 5.1 as described in Fig. 7. We also assume that water enters the rotor at the desired velocity and angle of attack to facilitate the evaluation and optimization process.

Rotational speed. Speed ratio, which is a dimensionless parameter, is defined as the ratio of the rotational speed to the nominal rotational speed ($\frac{N}{N_n}$) and is used here to display the results in a general sense. In order to optimize the value of speed ratio, it is changed from $\frac{1}{4}$ to $\frac{20}{11}$ and its effects on the efficiency and flow pattern inside the rotor are analyzed. The results of these simulations are plotted in Fig. 19; furthermore, velocity and pressure distribution inside the rotor for some of the cases are illustrated in Fig. 20 and Fig. 21, respectively.

Fig. 19 illustrates that the efficiency is parabolic in terms of speed ratio and the maximum efficiency occurs when the speed ratio is between 0.9 and 1. This is in accordance with Eq. 1 and experimental results of Mockmore [11] and numerous other studies. As can be seen from Fig. 19, there is a 15-percent difference between the hydraulic efficiency and the turbine efficiency, which is caused by that portion of the energy of the water that leaves the rotor. While the former efficiency only takes the losses inside the rotor into account, the latter also accounts for the unused energy of the water that exits the rotor, hence having a lower value.

At low rotational speeds the relative angle of the water jet with respect to the rotor is less than the blade inlet angle, causing flow separation on the suction side of the blades which results in a reduced efficiency. The same is true about high rotational speeds, only this time flow separation occurs on the pressure side of the blades and is illustrated in Fig. 22 for $\frac{N}{N_n} = \frac{10}{9}$. Note that even when the speed ratio is slightly higher than 1, flow separation occurs at the tip of the blades and the adverse

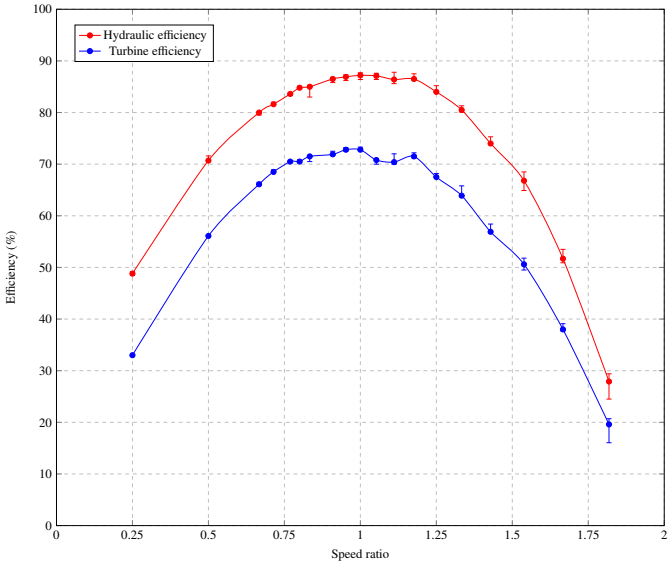

Figure 19: Plot of efficiency versus speed ratio. As predicted by Eq. 1, the curve is parabolic [11]. Hydraulic efficiency does not take the energy of the water that leaves the rotor into account, so it is higher than turbine efficiency.

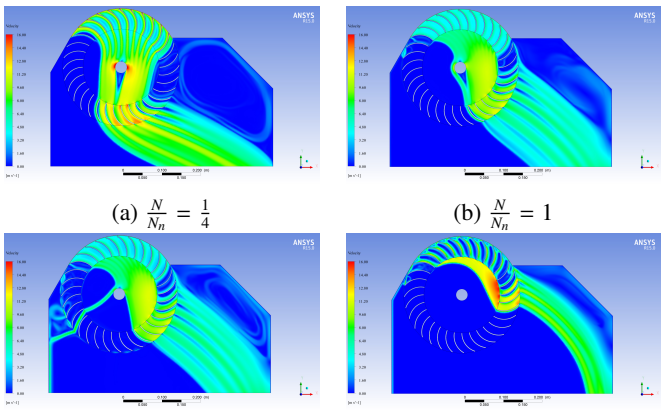

(a) $\frac{N}{N_n} = \frac{1}{4}$ (b) $\frac{N}{N_n} = 1$

(c) $\frac{N}{N_n} = \frac{10}{9}$ (d) $\frac{N}{N_n} = \frac{20}{11}$

Figure 20: Water velocity distribution inside the rotor for different speed ratios. As the speed ratio increases, water is deflected to the side of the rotor and away from the shaft. Very low or very high rotational speeds cause flow separation at the tip of the blades.

pressure gradient can result in undesirable effects such as cavitation [33].

Cross-Flow turbine is historically classified as an impulse-type turbine. However, Fig. 21 shows that the average relative static pressure of the water that enters the rotor is significantly higher than zero, leading to the conclusion that this turbine must be classified as a mixed-flow turbine [10, 21]. The average relative static pressure of water at the rotor entrance is plotted against the speed ratio in Fig. 23, and the curve illustrates a second-degree relationship between the two parameters. This static pressure is caused by the centrifugal acceleration imposed by the rotor and is further elaborated by Sammartano et al. [28].

Turbine efficiency reaches a maximum value of 72.8% when the speed ratio is 0.92, hence 0.92 is considered as the optimal value of the speed ratio and used in future steps to optimize

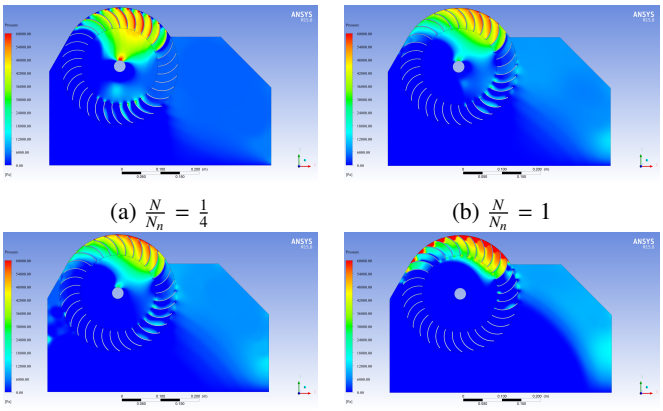

(a) $\frac{N}{N_n} = \frac{1}{4}$ (b) $\frac{N}{N_n} = 1$

(c) $\frac{N}{N_n} = \frac{10}{9}$ (d) $\frac{N}{N_n} = \frac{20}{11}$

Figure 21: Pressure distribution inside the rotor for different speed ratios. Relative static pressure at the core of the water jet is higher than the sides which are in contact with atmospheric pressure. Also, increasing the speed ratio increases the average relative static pressure at the rotor entrance because this pressure is directly proportional to the centrifugal acceleration imposed by the rotor [28].

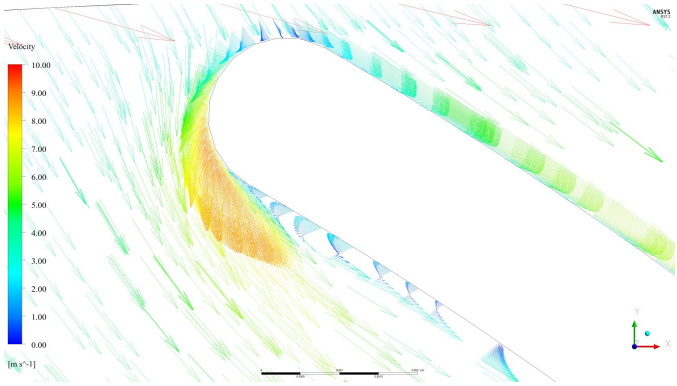

Figure 22: Velocity vectors entering the rotor for $\frac{N}{N_n} = \frac{10}{9}$. The vectors are drawn relative to a rotating frame of reference that has a rotational speed equal to that of the rotor. Note that even at speed ratios slightly higher than 1, flow separation can be observed on the pressure side of the blades.

other turbine parameters.

Angle of attack. The value of angle of attack is not optimized in this study because the 16 degree value, which is used here, has been the optimal value of angle of attack in numerous studies and is generally believed to yield the best results.

Admission angle. To optimize the value of admission angle, we changed it from 60 to 120 degrees and analyzed its effects on the efficiency and flow pattern inside the rotor. The results of these simulations are plotted in Fig. 24, and velocity and pressure distribution inside the rotor for some of the cases are shown in Fig. 25 and Fig. 26, respectively.

While the plot of turbine efficiency in Fig. 24 is mostly flat, the value obtained for an 80-degree admission angle is notably higher than other angles. To explain this result, note that:

- for angles greater than 80 degrees, a portion of the water that exits the first stage of the turbine strikes the rotor shaft which decreases turbine efficiency.

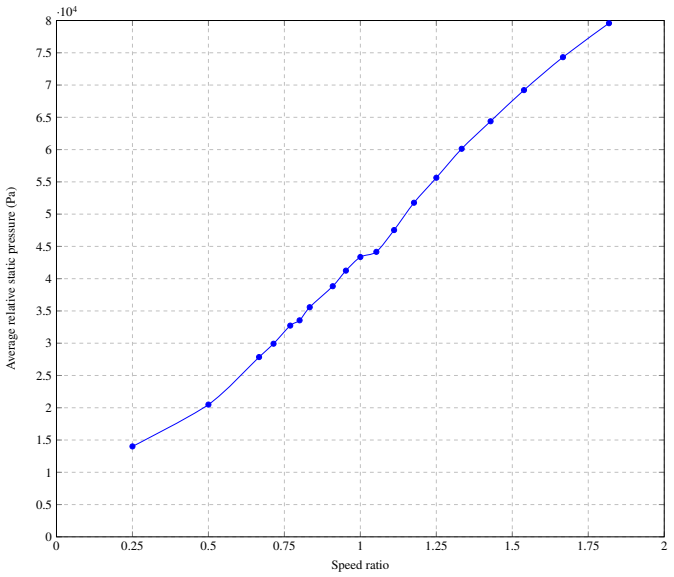

Figure 23: Plot of average relative static pressure at the rotor entrance versus speed ratio. The curve is parabolic because the pressure is directly proportional to the centrifugal acceleration imposed by the rotor [28].

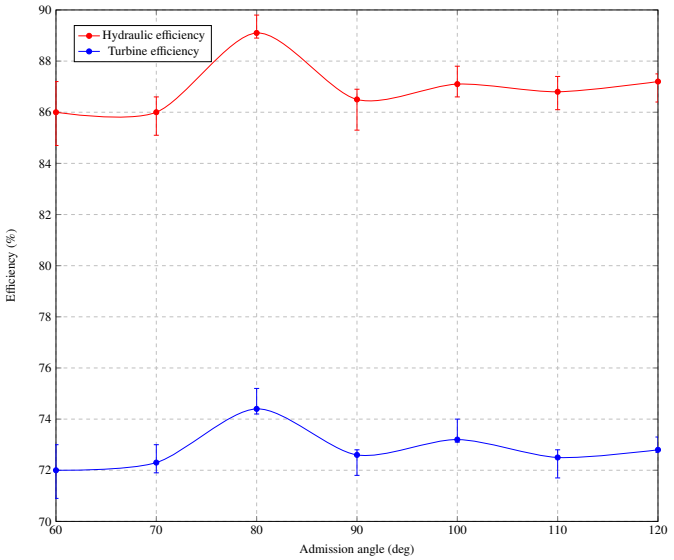

Figure 24: Plot of efficiency versus admission angle.

- As can be seen from Fig. 26, a static pressure gradient exists in the water jet that passes through the first stage of the turbine. This pressure is highest at the core of the jet and equal to the atmospheric pressure on the sides. As illustrated by Fig. 27, decreasing the admission angle narrows the entering water jet, reducing its relative static pressure and allowing the turbine to operate more closely to its ideal conditions.

- Decreasing the admission angle increases rotor length, which consequently increases water entrainment by the air that is trapped inside the housing when water passes through the middle of the rotor. Therefore, it results in the loss of efficiency [34].

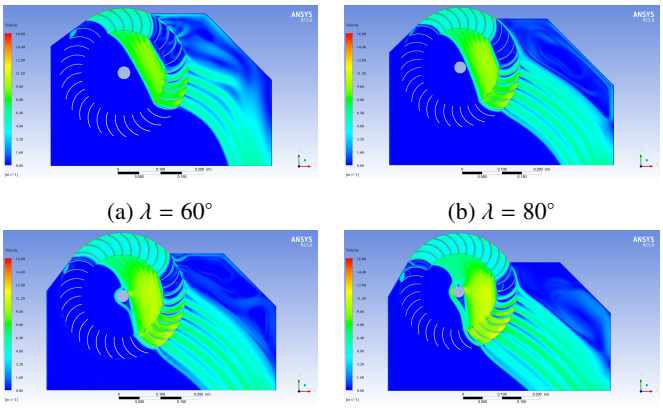

(a) $\lambda = 60°$ (b) $\lambda = 80°$

(c) $\lambda = 100°$ (d) $\lambda = 120°$

Figure 25: Water velocity distribution inside the rotor for different admission angles. As the admission angle increases, the water jet becomes wider and eventually strikes the shaft.

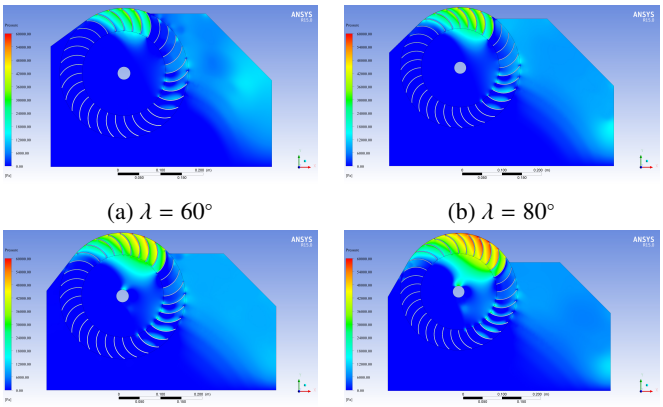

(a) $\lambda = 60°$ (b) $\lambda = 80°$

(c) $\lambda = 100°$ (d) $\lambda = 120°$

Figure 26: Pressure distribution inside the rotor for different admission angles. As the admission angle increases, the relative static pressure at the core of the water jet increases, and so does the average value at the rotor entrance.

When the admission angle is 80 degrees, turbine efficiency becomes 74.4% and a balance is achieved between the three aforementioned effects. Therefore, 80 degrees is selected as the optimal value of admission angle and used in future steps.

Blade profile. The initial design of the blades is simply a circular arc with constant thickness with rounded ends, as shown in Fig. 28a. It is then optimized according to the following guidelines:

- the blade tip that faces the entering water must be as small as possible to avoid efficiency losses due to friction; however, it should not be wedge-shaped because although a wedge-shaped blade performs best at design point conditions, at slightly off-design conditions it has the tendency for flow separation on one side that results high losses.

- The blade must be shaped like an airfoil in order to utilize the higher than zero relative static pressure at the rotor entrance.

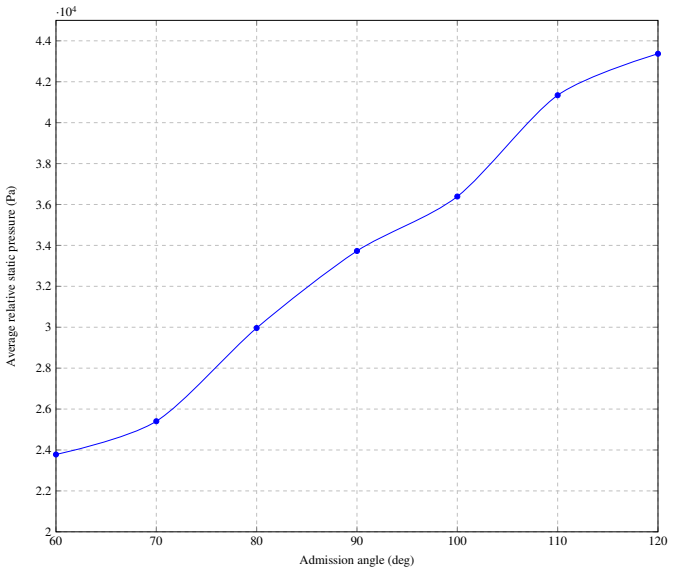

Figure 27: Plot of average relative static pressure at the rotor entrance versus admission angle. Increasing the admission angle and widening the water jet increases the average relative static pressure at the rotor entrance.

- The other end of the blade must be small as well in order to limit the wake in the exiting flow from the first stage and prevent losses due to friction for the entering water to the second stage.

Following these guidelines, the optimal blade profile is shown in Fig. 28b which increases turbine efficiency to 77.4%.

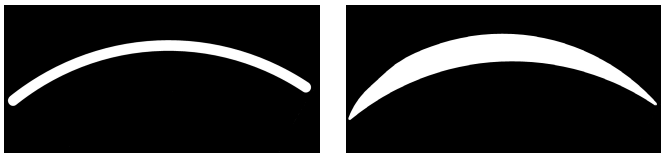

(a) initial design (b) final design

Figure 28: Initial and final designs of the blade profile. The final profile utilizes the above zero relative static pressure at the rotor entrance and has the minimum amount of resistance for the incoming and outgoing flows.

Diameter ratio. To optimize the value of diameter ratio, it is changed from 0.58 to 0.74 and its effects on the efficiency and flow pattern inside the rotor are evaluated. The results of these simulations are shown in Fig. 29. Additionally, velocity and pressure distribution inside the rotor for some of the cases are illustrated in Fig. 30 and Fig. 31, respectively.

Fig. 29 illustrates that the turbine efficiency is parabolic in terms of diameter ratio and the maximum value is achieved when diameter ratio is equal to 0.68. This can be attributed to the following factors:

- increasing the diameter ratio consequently increases the tangential component of flow velocity at the inner blade tips, which deflects velocity vectors away from the shaft.

- As shown in Fig. 31 and further illustrated in Fig. 32, increasing the diameter ratio reduces the amount of built-

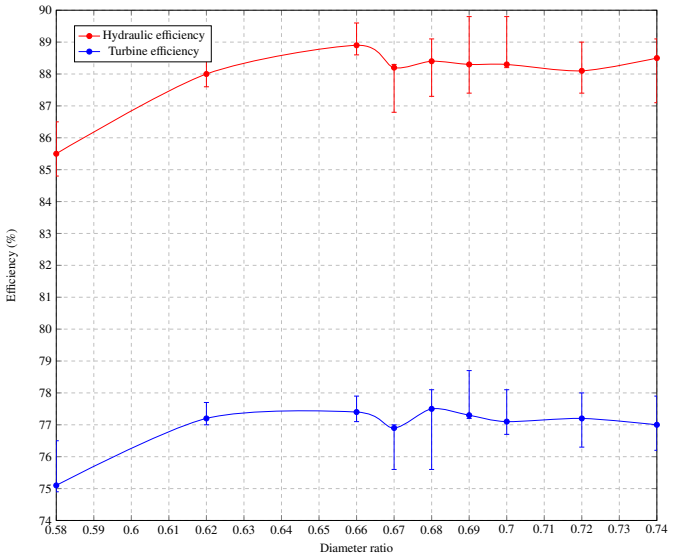

Figure 29: Plot of efficiency versus diameter ratio. The turbine efficiency is approximately constant for diameter ratios between 0.62 and 0.72, with the maximum value happening at 0.68.

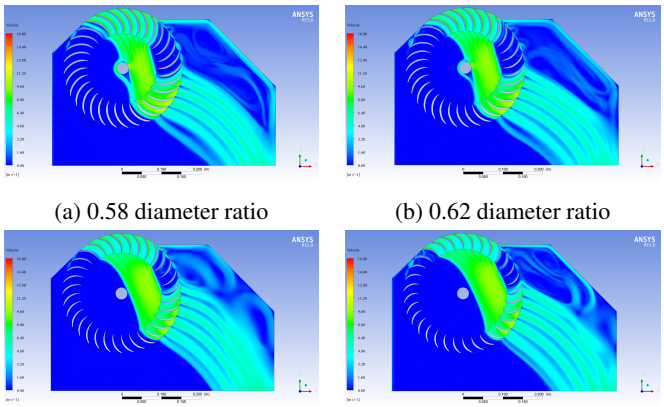

(a) 0.58 diameter ratio (b) 0.62 diameter ratio

(c) 0.68 diameter ratio (d) 0.74 diameter ratio

Figure 30: Water velocity distribution inside the rotor for different diameter ratios. Increasing the diameter ratio changes the position and the tangential component of the velocity of the water that exits the first stage of the turbine and translates the flow.

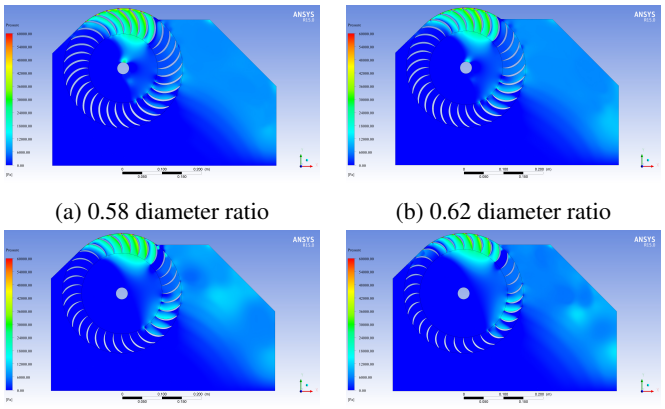

(a) 0.58 diameter ratio (b) 0.62 diameter ratio

(c) 0.68 diameter ratio (d) 0.74 diameter ratio

Figure 31: Pressure distribution inside the rotor for different diameter ratios. Increasing the diameter ratio reduces the amount of built-up back-pressure at the rotor entrance and consequently the average relative static pressure [28].

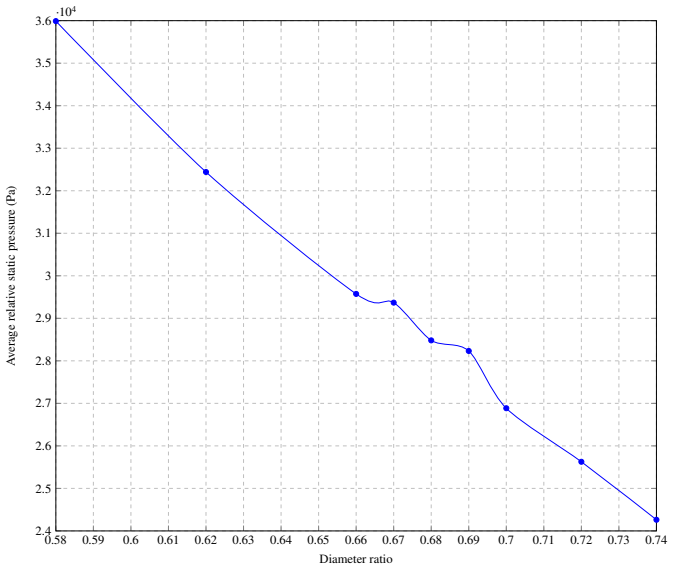

Figure 32: Plot of average relative static pressure at rotor entrance versus diameter ratio. Increasing the diameter ratio reduces the amount of built-up back-pressure at the rotor entrance and consequently the average relative static pressure [28].

up back-pressure at the rotor entrance and consequently the average relative static pressure [28]. As explained previously, this increases efficiency.

- Increasing the diameter ratio reduces the length of the blade. Aside from reducing the time for water to transfer its energy to the blades, the blade curvature is increased amplifying the associated losses.

When the value of diameter ratio is 0.68, turbine efficiency reaches a maximum value of 77.5%. This diameter ratio maintains a good balance between the aforementioned effects and is also in good agreement with the theoretical value of 0.657 which was calculated previously. Therefore, it is selected as the optimal diameter ratio and used in future steps.

Number of blades. We changed the number of blades from 24 to 40 and analyzed its effects on the efficiency and flow pattern inside the rotor. The results of these simulations are plotted in Fig. 33. Furthermore, total pressure distribution inside the rotor for some of the cases are shown in Fig. 34.

Increasing the number of blades increases the area of energy transfer to the rotor and reduces the volume of semi-filled blade channels on the sides of the admission arc [28]; however, increasing the number of blades increases the total solid thickness that blocks the incoming water jet and reduces the equivalent hydraulic diameter of each blade channel which increases flow losses. As illustrated by Fig. 33, a balance is achieved between these effects for 35 blades and the efficiency reaches a maximum value of 78.6%; therefore, 35 is selected as the optimal value for the number of blades.

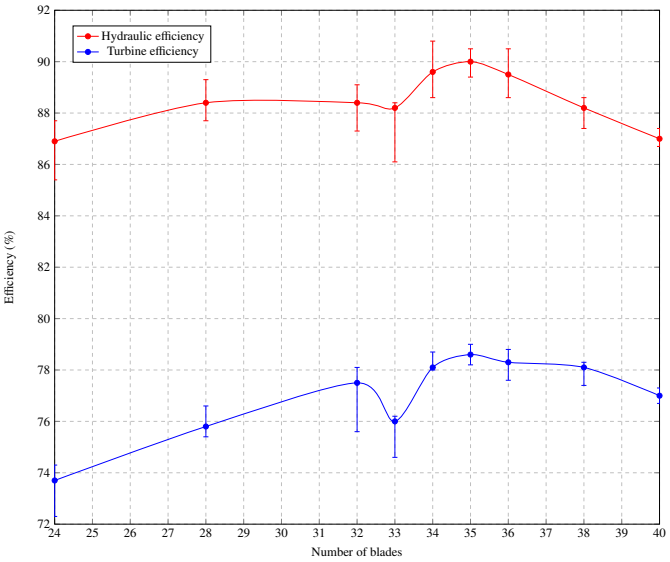

Figure 33: Plot of efficiency versus the number of blades. Turbine efficiency is nearly parabolic in terms of the number of blades and the maximum value is achieved for 35 blades.

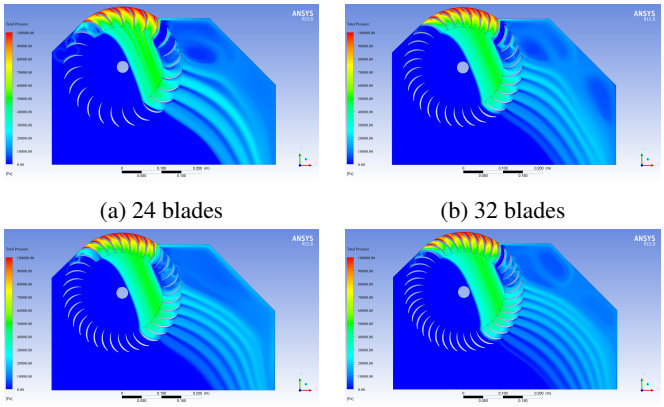

(a) 24 blades (b) 32 blades

(c) 35 blades (d) 40 blades

Figure 34: Total pressure distribution inside the rotor for different number of blades. Increasing the number of blades increases the area of energy transfer to the rotor and reduces the volume of semi-filled blade channels on the sides of the admission arc [28]. About $\frac{2}{3}$ of the amount of output power is transferred to the rotor during the first stage of the turbine, while the rest is transferred during the second stage [11].

Fig. 33 illustrates that turbine efficiency is parabolic in terms of the number of blades; however, the value obtained for 33 blades seems unfitting to the rest of the data. As explained previously in sec. 4.2.3, this is caused by using the Frozen Rotor frame change model, because this model does not account for the relative position of the rotor blades and the admission arc.

Summary. The optimal values obtained for turbine parameters are tabulated in Tab. 6, along with their contribution to increasing the efficiency. Alongside optimizing these parameters, modifying the blade profile made the largest contribution to the efficiency, increasing it by 3.1%. Overall, the efficiency was increased by 5.9%. The values in Tab. 6 mostly agree with the results of previous studies in Tab. 1.

Table 6: Optimal values of turbine parameters. Blade profile, which made the biggest contribution to the efficiency, is not listed in this table.

Turbine parameter	Value	Efficiency increase (%)
speed ratio	0.92	-
angle of attack (deg)	16	-
admission angle (deg)	80	1.6
diameter ratio	0.68	0.1
number of blades	35	1.1

5.2.3. *Third step*

In the final step, the optimal nozzle and rotor are joined together and the resulting turbine is simulated under various load conditions and modified as necessary to achieve constant efficiency over a wide range of operating conditions (the nozzle geometry is slightly modified to reflect the 80-degree value of admission angle). To that end, the guide vane angle is changed and the performance of the turbine is evaluated under constant head, variable flow rate conditions. The results of these simulations for single- and multi-cell turbines are plotted in terms of flow ratio (the ratio of volume flow rate to nominal volume flow rate) in Fig. 35 and Fig. 36, respectively. Furthermore, water velocity distribution for some of the cases is shown in Fig. 37.

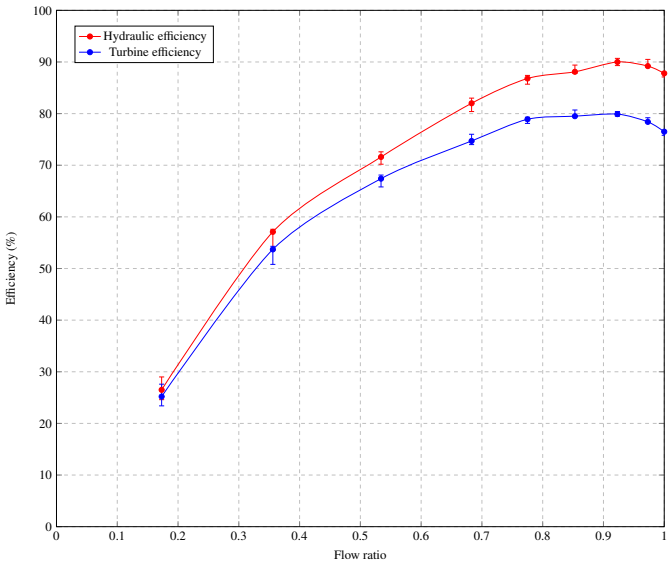

Figure 35: Plot of efficiency versus flow ratio for the initial single-cell turbine design. The turbine operates well for flow ratios between 0.775 and 1, but the efficiency decreases for lower flow ratios due to detachment of water from the lower surface of the guide vane.

As can be seen from Fig. 35, although turbine efficiency is approximately constant for flow ratios between 0.775 and 1, its value drops steadily for flow ratios below that limit. This is caused by the increase in nozzle losses and the improper entrance of the lower water jet to the rotor.

As the guide vane angle decreases, the shape of the channel below the guide vane transforms from a nozzle into a diffuser, which causes the lower water jet to detach from the guide vane surface. This portion of the water jet partially enters the rotor

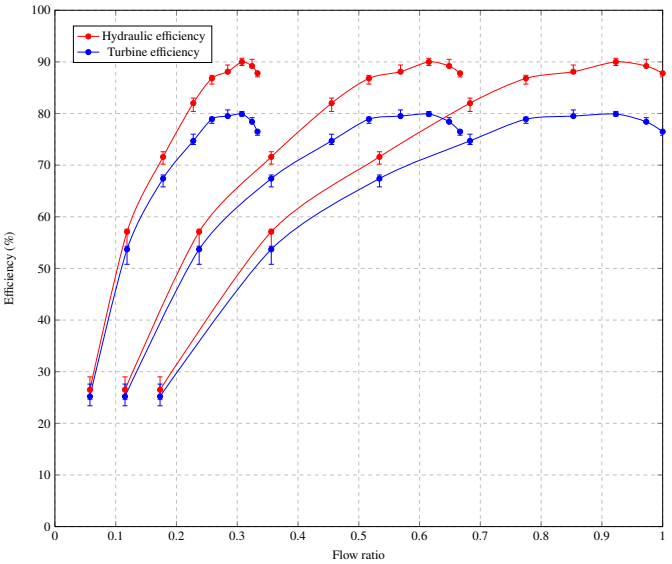

Figure 36: Plot of efficiency versus flow ratio for the initial multi-cell turbine design. The turbine has a 1:2 division to handle low flow conditions. The graph suggests that the turbine will face drops in efficiency for low flow conditions.

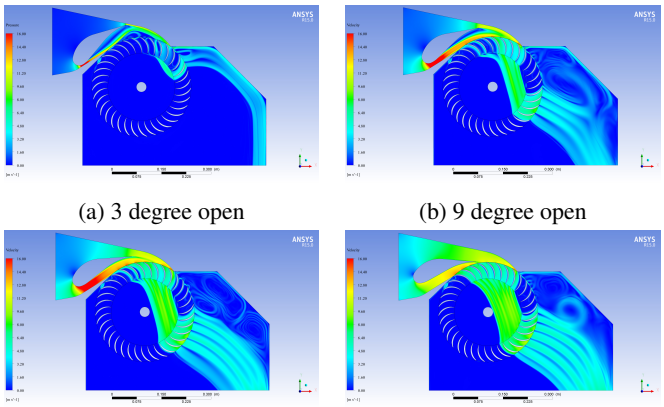

(a) 3 degree open (b) 9 degree open

(c) 15 degree open (d) 24 degree open

Figure 37: Water velocity distribution inside the initial turbine design for different guide vane angles. For small guide vane angles, there is an abrupt increase in water velocity and the stream that passes below the guide vane gets detached from its surface, resulting in loss of efficiency.

and the rest of it travels in the space above the rotor until it merges with the upper water jet. This effect increases nozzle losses dramatically and results in significant loss of efficiency.

To alleviate this problem, the geometry of the channel below the guide vane is redesigned so that it can maintain the shape of a nozzle even in small guide vane angles; however, in the new design geometrical constraints required the admission angle to be increased to 110 degrees. The performance of the modified turbine is evaluated, and the results of these simulations for single- and multi-cell turbines are plotted in Fig. 38 and Fig. 39, respectively. Moreover, water velocity and pressure distribution and plots of velocity and angle of attack profiles at the rotor entrance for some of the cases are shown in Fig. 40 to Fig. 43, respectively.

As can be seen from Fig. 40, in the new design the lower

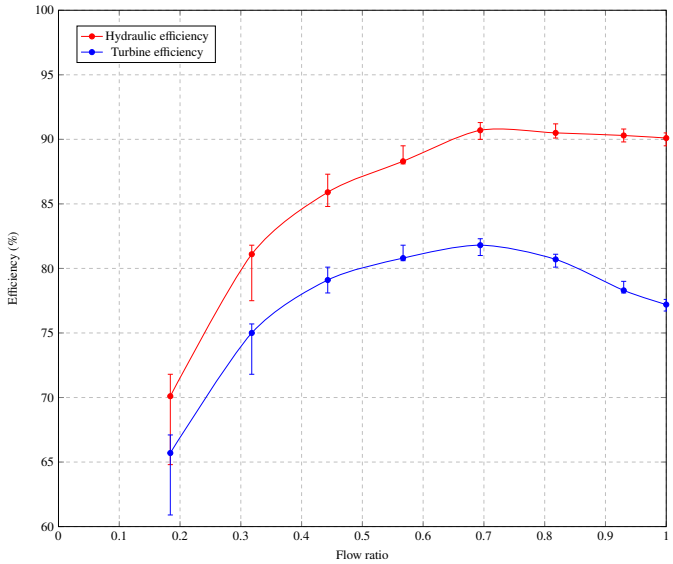

Figure 38: Plot of efficiency versus flow ratio for the final single-cell turbine design. The drop in efficiency is less compared to the initial design and it is approximately constant for a wide range of flow ratios. Maximum efficiency is achieved for an opening of 15 degrees which corresponds to a flow ratio of 0.69.

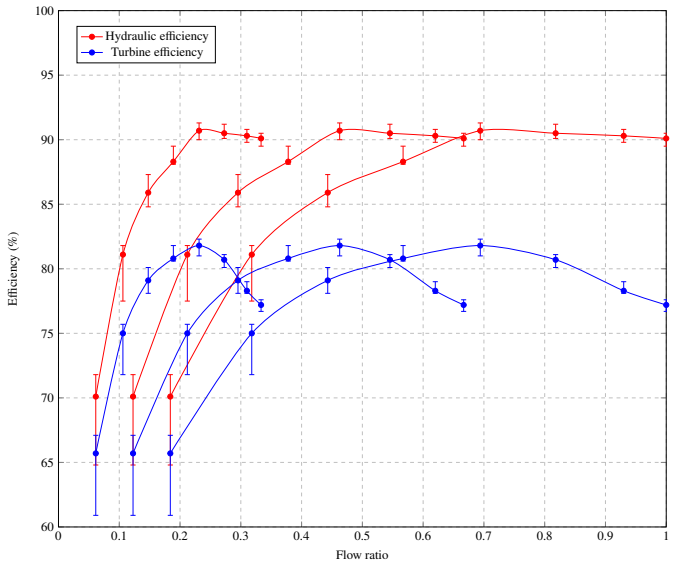

Figure 39: Plot of efficiency versus flow ratio for the final multi-cell turbine design. While the value of turbine efficiency is above 80% for a wide range of flow ratios, the final design of the multi-cell turbine can guarantee an efficiency value of approximately 78% for flow ratios higher than 0.16.

water jet is attached to the guide vane surface even for small guide vane angles. This results in a huge reduction in nozzle losses and boosts turbine efficiency, as shown by Fig. 38. Furthermore, Fig. 39 illustrates that a multi-cell turbine can maintain an approximate efficiency value of 78% for flow ratios from 0.16 to 1. Moreover, it can be seen from Fig. 42 and Fig. 43 that velocity and angle of attack profiles are approximately uniform for the water jet that enters the rotor (aside from the ripples caused by stagnation points on blade tips) which further validates the process used to design the nozzle geometry.

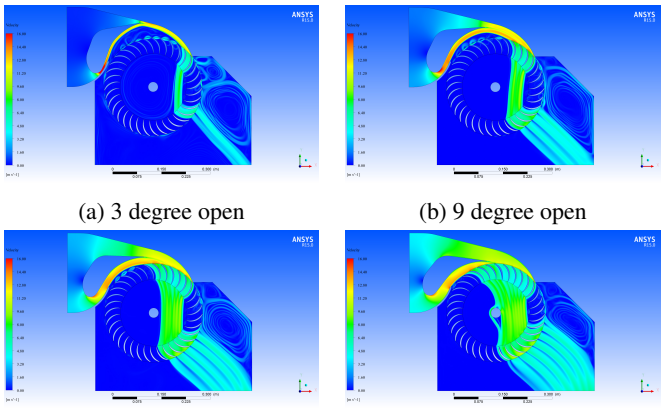

(a) 3 degree open (b) 9 degree open

(c) 15 degree open (d) 21 degree open

Figure 40: Water velocity distribution inside the final turbine design for different guide vane angles. Note that the lower water jet is attached to the lower surface of the guide vane even for small angles.

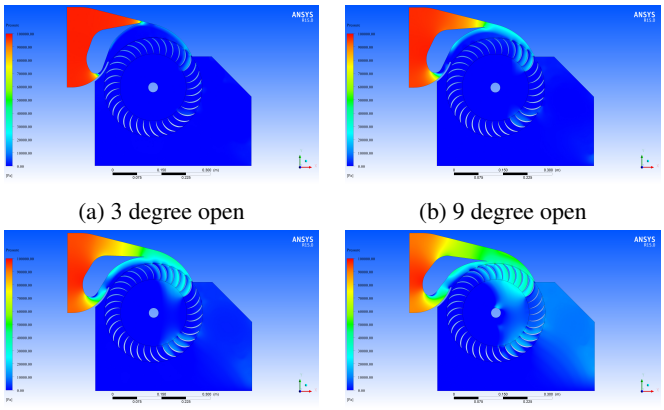

(a) 3 degree open (b) 9 degree open

(c) 15 degree open (d) 21 degree open

Figure 41: Pressure distribution inside the final turbine design for different guide vane angles.

In the final step, guide vane angle is held constant at 15 degrees (corresponding to the maximum value of turbine efficiency) and water head is changed by as much as 40% to evaluate the performance of the turbine. The results of these simulations are plotted in terms of head ratio (the ratio of water head to nominal water head) in Fig. 44.

Fig. 44 illustrates that the efficiency is approximately constant for high head ratios, but slightly drops for head ratios below 0.9. This can be attributed to the blade profile used which can handle a range of incoming flow angles without resulting in flow separation and a drop in efficiency.

Finally, to get an overview of the performance of the single-cell turbine, data from Fig. 38 and Fig. 44 are combined to plot the normalized Hill Chart diagram of the turbine shown in Fig. 45. Note that for a wide range of operating conditions, the single-cell turbine guarantees an efficiency value of 77% and a maximum value of 81.8%, and this range can be expanded if a multi-cell turbine is used. Overall, Fig. 45 shows that the proposed methodology can be successfully implemented to design a low-cost, high-performance Cross-Flow turbine.

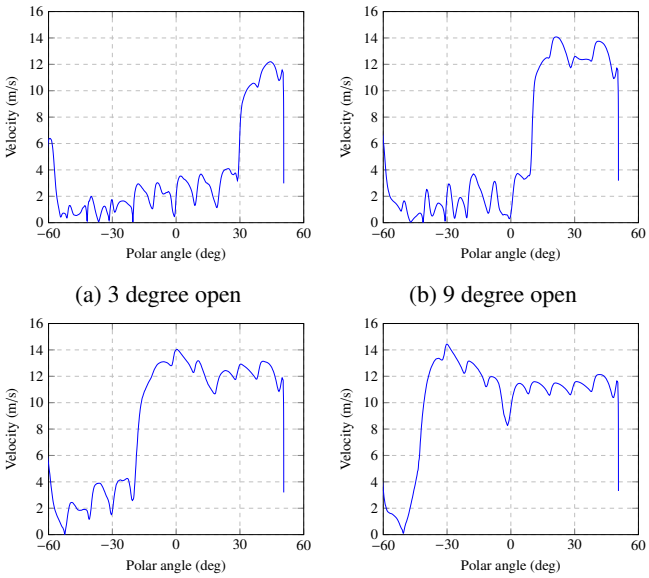

(a) 3 degree open (b) 9 degree open

(c) 15 degree open (d) 21 degree open

Figure 42: Velocity profiles at the rotor entrance of the final turbine design for different guide vane angles.

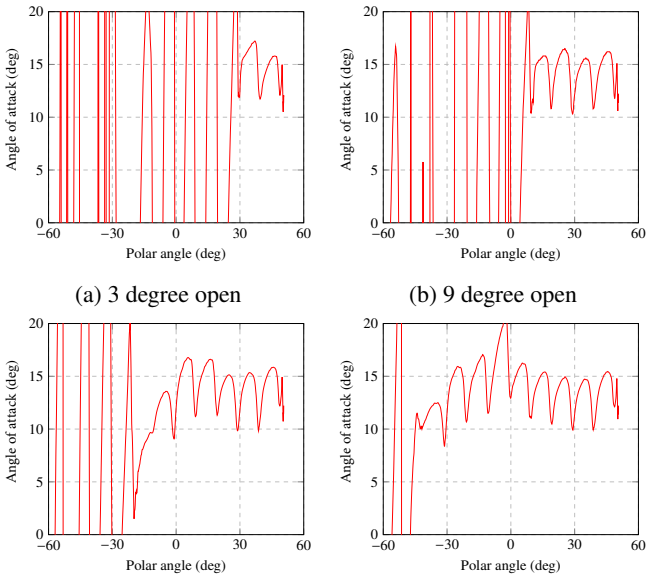

(a) 3 degree open (b) 9 degree open

(c) 15 degree open (d) 21 degree open

Figure 43: Angle of attack profiles at the rotor entrance of the final turbine design for different guide vane angles.

5.2.4. *Numerical accuracy*

Aside from validating the CFD model by experimental data which was discussed in subsubsec. 4.2.3, several other measures are used to verify the numerical accuracy of the results.

Meshing quality is one of the most important factors in obtaining accurate results, hence various parameters that represent the quality of the mesh were constantly checked before the start of the simulation. Aspect ratio, skewness and orthogonal quality are among the most important of these parameters, and their average values in the simulations are reported in Tab. 7. As can

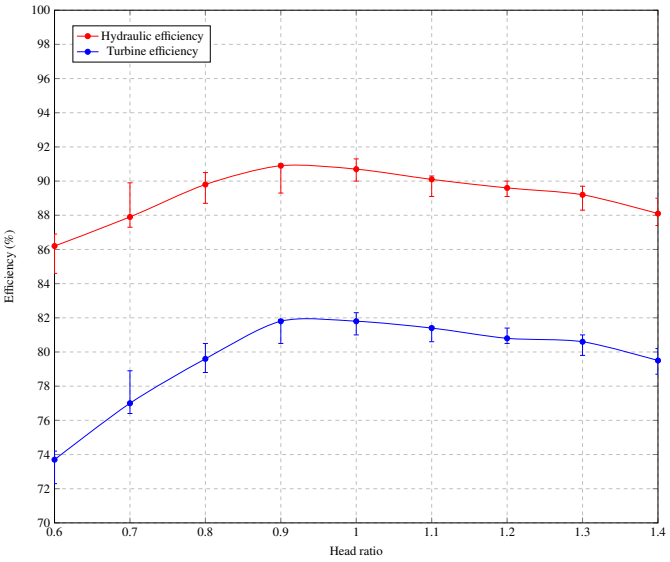

Figure 44: Plot of efficiency versus head ratio for the final turbine design.

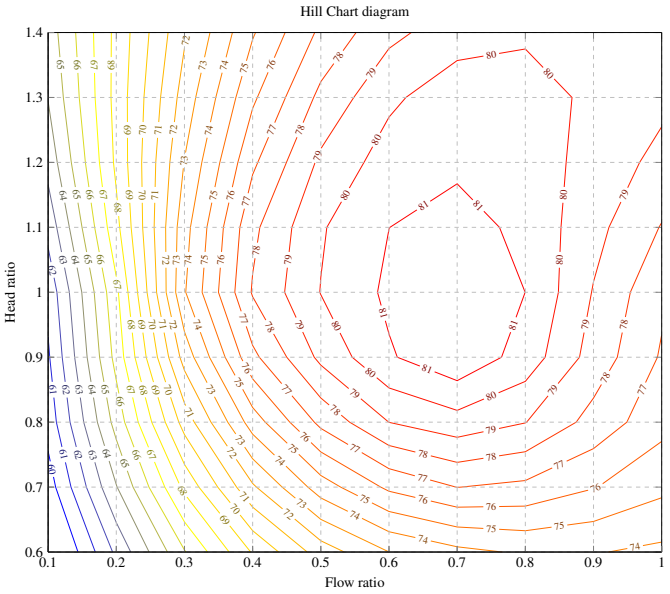

Figure 45: Normalized Hill Chart diagram of the final turbine design. For a wide range of operating conditions, the single-cell turbine guarantees an efficiency value of 77% and a maximum value of 81.8%, and this range can be expanded if a multi-cell turbine is used.

be seen from Tab. 7, all of these values are in the recommended intervals [77].

Table 7: Average values of mesh quality parameters for nozzle, rotor and turbine simulations. The slightly high average value of aspect ratio is due to the long, narrow prismatic elements that form the inflation layers.

Region	Aspect ratio	Skewness	Orthogonal quality
nozzle	8.0	0.35	0.81
rotor	28.5	0.32	0.81
turbine	11.6	0.35	0.81

Simulations were continued until residuals decreased by at least 3 orders of magnitude to ensure the results had 3 significant figures. Furthermore, equation imbalances were monitored to verify that they were well below the recommended threshold of 1%. The maximum value of these imbalances for nozzle, rotor and turbine simulations were 0.0001%, 0.2951% and 0.3249%, respectively.

After each simulation, the average value of y^+ on each of the solid surfaces was checked to ensure it was lower than the recommended value of 11.06 [73]. The average and maximum values of y^+ in the simulations are tabulated in Tab. 8.

Table 8: Average and maximum values of y^+ on solid surfaces. The recommended average value for a high-quality boundary layer resolution is 11.06 [73].

Region	Surface	Average value	Maximum value
nozzle	walls	4.98	8.32
rotor	blades	2.41	9.58
	shaft	2.41	3.62
	housing	2.08	13.74
turbine	blades	1.80	8.28
	shaft	0.64	1.57
	housing	1.27	6.59
	nozzle	3.81	7.19
	guide vane	3.91	8.31

Finally, it is worthwhile to check the grid (spatial) independence of the results. To do this, values of local and global parameters were monitored as the meshing was refined until all of the values converged to a final target. This is shown for the nozzle in Fig. 46 and Fig. 47 as an example. Water velocity at three different points is selected as the local variable and nozzle loss coefficient is chosen as the global variable.

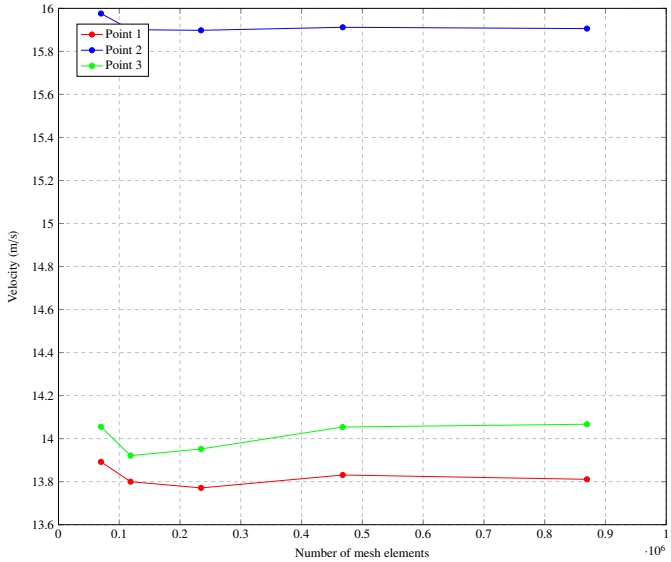

Figure 46: Grid independence of local variables for nozzle simulations. All three variables converge when the number of mesh elements passes 500000.

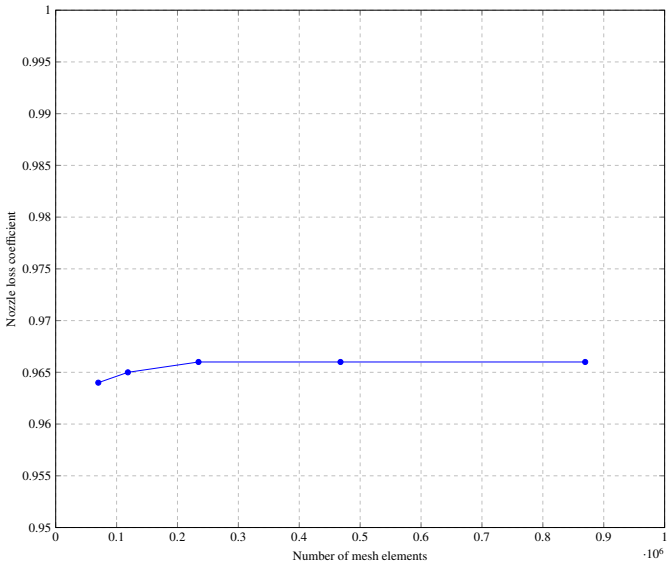

Figure 47: Grid independence of a global variable for nozzle simulations. Nozzle loss coefficient converges when the number of mesh elements passes 200000.

6. Conclusion

In this article an extensive review on the research conducted on Hydraulic Cross-Flow turbine was provided. It was found that inconsistencies exist in the results and a universal, coherent design methodology is needed. To address this issue, we introduced a new design framework, both for the system-level and detail design phases. In the system-level design phase, we used theoretical expressions and experimental data to obtain the values of key turbine parameters such as rotor diameter. In the detail design phase, we introduced a three-step process based on numerical simulations to design and optimize the geometry of the turbine and evaluate its performance. The CFD model was validated using experimental data from a prototype Cross-Flow turbine.

The proposed scheme was used to design a high-efficiency, low-cost Cross-Flow turbine. Various turbine parameters, including speed ratio, blade profile and the number of blades were optimized for obtaining the highest efficieny. Finally, we evaluated the performance of the turbine under various operating conditions. The single-cell turbine that we designed guarantees an efficiency value of 77% for a wide range of load conditions and a maximum value of 81.8%. This range can be expanded if a multi-cell turbine is used.

Acknowledgment

The authors wish to express their gratitude to WRI for permission to use its testing facility, and to Iran Water and Power Resources Development Company (IWPCO) and Sharif University of Technology for supporting the project.

Funding: Financial support for designing the prototype turbine and performing the experiments was provided by WRI and IWPCO. Experimental tests were carried out at the testing facility of WRI. Financial support for research on a new design methodology and performing numerical simulations was provided by DSDA. WRI, IWPCO or DSDA did not have any role in study design; in the collection, analysis and interpretation of data; in the writing of the report; and in the decision to submit this article for publication.

List of symbols

Greek symbols

α Attack angle (deg, rad)
β Blade tip angle (deg, rad)
Δ Uncertainty amount
δ Blade central angle (deg, rad)
η Efficiency
λ Admission angle (deg, rad)
ρ Density (kg/m^3)
Radius (m)
ψ Rotor loss coefficient
ω Rotational speed (rad/s)

Latin symbols

B Rotor length (m)
C Coefficient
D Rotor diameter (m)
g Gravitational acceleration (m/s^2)
H Water head (m)
N Rotational speed (rpm)
N′ Specific speed
P Power (W)
Q Water volume flow rate (m^3/s)
R Rotor radius (m)
S Nozzle height (m)
U Blade tip linear velocity (m/s)
V Absolute water velocity (m/s)

Subscripts

b Blade
e Exit
g Generator
h Hydraulic
i Input
l Loss
m Mechanical transmission system
n Nozzle
o Output
q Modified
s Dimensionless
sd Metric
t Turbine

References

References

[1] Williamson SJ, Stark BH, Booker JD. Low-Head Pico Hydro Turbine Selection Using a Multi-Criteria Analysis. Renew Energy 2014;61:43-50.

[2] Based on IEA data from the Key Renewables Trends OECD/IEA 2016. Licence: www.iea.org/t&c; as modified by the authors.
[3] Paish O. Micro-Hydropower: Status and Prospects. Proc of the Inst of Mech Eng, Part A: J Power Energy 2002;216.1:31-40.
[4] Banos R, Manzano-Agugliaro F, Montoya FG, Gil C, Alcayde A, Gomez J. Optimization Methods Applied to Renewable and Sustainable Energy: A Review. Renew Sustain Energy Rev 2011;15.4:1753-66.
[5] Weijermars R, Taylor P, Bahn O, Das SR, Wei Y. Review of Models and Actors in Energy Mix Optimization - Can Leader Visions and Decisions Align with Optimum Model Strategies for Our Future Energy Systems?. Energy Strategy Rev 2012;1.1:5-18.
[6] Mohibullah M, Radzi AM, Hakim MIA. Basic Design Aspects of Micro Hydro Power Plant and its Potential Development in Malaysia. Power Energy Conf, 2004. PECon 2004. Proc. Natl.
[7] Costa Pereira NH, Borges JE. Study of the Nozzle Flow in a Cross-Flow Turbine. Int J Mech Sci 1996;38.3:283-302.
[8] Ossberger GmbH + Co. The OSSBERGER Turbine, http://www.ossberger.de/cms/en/hydro/the-ossberger-turbine-for-asynchronous-and-synchronous-water-plants/; 2016 [accessed 16.10.16].
[9] Office of Energy Efficiency and Renewable Energy, U.S. Department of Energy. Types of hydropower plants, http://energy.gov/eere/water/types-hydropower-plants#sizes; 2016 [accessed 13.09.16].
[10] Sammartano V, Arico C, Carravetta A, Fecarotta O, Tucciarelli T. Banki-Michell Optimal Design by Computational Fluid Dynamics Testing and Hydrodynamic Analysis. Energies 2013;6.5:2362-85.
[11] Mockmore CA, Merryfield F. The Banki Water Turbine. Engineering Experiment Station Bulletin Series Number 25, Oregon State System of Higher Education, Oregon State College, Corvallis, February 1949.
[12] Durali M. Design of Small Water Turbines for Farms and Small Communities. Department of Mechanical Engineering, Massachusetts Institute of Technology, Cambridge, MA, 1976.
[13] Khosrowpanah S, Fiuzat AA, Albertson ML. Experimental Study of Cross-Flow Turbine. J Hydraul Eng 1988;114.3:299-314.
[14] The Original OSSBERGER^{TM} Cross-Flow Turbine, http://www.ossberger.de/cms/fileadmin/user_upload/1-2-02.pdf; June 2016 [accessed 13.09.16].
[15] Fiuzat AA, Akerkar BP. Power Outputs of Two Stages of Cross-Flow Turbine. J Energy Eng 1991;117.2:57-70.
[16] Aziz NM, Desai VR. An Experimental Study of the Effect of Some Design Parameters on Cross-Flow Turbine Efficiency. Eng Rep, Department of Civil Engineering, Clemson University, 1991.
[17] Desai VR, Aziz NM. An Experimental Investigation of Cross-Flow Turbine Efficiency. J Fluids Eng 1994;116.3:545-50.
[18] Olgun H. Investigation of the Performance of a Cross-Flow Turbine. Int J Energy Res 1998;22.11:953-64.
[19] Olgun H. Effect of Interior Guide Tubes in Cross-Flow Turbine Runner on Turbine Performance. Int J Energy Res 2000;24.11:953-64.
[20] Kaunda CS, Kimambo CZ, Nielsen TK. Experimental Study on a Simplified Cross-Flow Turbine. Int J Energy Environ 2014;5.2:155-82.
[21] Kaunda, CS, Kimambo CZ, Nielsen TK. A Numerical Investigation of Flow Profile and Performance of a Low-Cost Cross-Flow Turbine. Int J Energy Environ 2014;5.3:275-96.
[22] Choi YD, Lim JI, Kim YT, Lee YH. Performance and Internal Flow Characteristics of a Cross-Flow Hydro Turbine by the Shapes of Nozzle and Runner Blade. J Fluid Sci Technol 2008;3.3:398-409.
[23] Choi YD, Shin BR, Lee YH. Air Layer Effect on the Performance Improvement of a Cross-Flow Hydro Turbine. J Fluid Mach 2010;13.4:37-43.
[24] Choi YD, Son SW. Shape Effect of Inlet Nozzle and Draft Tube on the Performance and Internal Flow of Cross-Flow Hydro Turbine. J Korean Soc Mar Eng 2012;36.3:351-7.
[25] Kokubu K, Kanemoto T, Son SW, Choi YD. Performance Improvement of a Micro Eco Cross-Flow Hydro Turbine. J Korean Soc Mar Eng 2012;36.7:902-9.
[26] Chen Z, Choi YD. Influence of Air Supply on the Performance and Internal Flow Characteristics of a Cross-Flow Turbine. Renew Energy 2015;79:103-10.
[27] De Andrade J, Curiel C, Kenyery F, Aguillon O, Vasquez A, Asuaje M. Numerical Investigation of the Internal Flow in a Banki Turbine. Int J Rotating Mach 2011:841214.
[28] Sammartano V, Morreale G, Sinagra M, Collura A, Tucciarelli T. Experimental Study of Cross-Flow Micro Turbines for Aqueduct Energy Recovery. Procedia Eng 2014;89:540-7.
[29] Sammartano V, Arico C, Sinagra M, Tucciarelli T. Cross-Flow Turbine Design for Energy Production and Discharge Regulation. J Hydraul Eng 2014;141.3:04014083.
[30] Sinagra M, Sammartano V, Arico C, Collura A, Tucciarelli T. Cross-Flow Turbine Design for Variable Operating Conditions. Procedia Eng 2014;70:1539-48.
[31] Sinagra M, Sammartano V, Arico C, Collura A. Experimental and Numerical Analysis of a Cross-Flow Turbine. J Hydraul Eng 2015;142.1:04015040.
[32] Yassen SR. Optimization of the Performance of Micro Hydro-Turbines for Electricity Generation. University of Hertfordshire, Hatfield, UK, May 2014.
[33] Adhikari RC, Vaz J, Wood D. Cavitation Inception in Cross-Flow Hydro Turbines. Energies 2016;9.4:237.
[34] Durgin WW, Fay WK. Some Fluid Flow Characteristics of a Cross-Flow Type Hydraulic Turbine. Proc Am Soc Mech Eng (ASME), Annu Winter Meet Small Hydropower Fluid Mach, New Orleans, LA, 1984.
[35] Fukutomi J, Nakase Y, Watanabe T. A Numerical Method of Free Jet from a Cross-Flow Turbine Nozzle. Bulletin Jpn Soc Mech Eng (JSME) 1985;28.241:1436-40.
[36] Totapally HGS, Aziz NM. Refinement of Cross-Flow Turbine Design Parameters. J Energy Eng 1994;120.3:133-47.
[37] Joshi CB, Seshadri V, Singh SN. Parametric Study on Performance of Cross-Flow Turbine. J Energy Eng 1995;121.1:28-45.
[38] Reddy H, Seshadri V, Kothari DP. Effect of Draft Tube Size on the Performance of a Cross-Flow Turbine. Energy Sources 1996;18.2:143-9.
[39] Kaniecki M. Modernization of the Outflow System of Cross-Flow Turbines. Task Q 6 2002;601-8.
[40] Kaniecki M, Steller J. Flow Analysis through a Reaction Cross-Flow Turbine. Proc Conf Model Fluid Flow (CMFF) 2003;3.
[41] Walseth EC. Investigation of the Flow through the Runner of a Cross-Flow Turbine. Department of Energy and Process Engineering, Norwegian University of Science and Technology, 2009.
[42] Haurissa J, Wahyudi S, Irawan YS, Soenoko R. The Cross-Flow Turbine Behavior towards the Turbine Rotation Quality, Efficiency, and Generated Power. J Appl Sci Res 2012;8.1:448-53.
[43] Kokubu K, Kanemoto T, Yamasaki K. Guide Vane with Current Plate to Improve Efficiency of Cross-Flow Turbine. Open J Fluid Dyn 2013;3.2:28-35.
[44] Reihani A, Ojaghi A, Derakhshan S, Beigzadeh B. Shaft Fatigue Life and Efficiency Improvement of a Micro Cross-Flow Turbine. Eng Solid Mech 2014;2.1:1-14.
[45] Acharya N, Kim CG, Thapa B, Lee YH. Numerical Analysis and Performance Enhancement of a Cross-Flow Hydro Turbine. Renew Energy 2015;80:819-26.
[46] Elbatran AH, Yaakob OB, Ahmed YM, Shabara HM. Operation, Performance and Economic Analysis of Low-Head Micro-Hydropower Turbines for Rural and Remote Areas: A Review. Renew Sustain Energy Rev 2015;43:40-50.
[47] Elbatran AH, Yaakob OB, Ahmed YM, Jalal MR. Novel Approach of Bidirectional Diffuser-Augmented Channels System for Enhancing Hydrokinetic Power Generation in Channels. Renew Energy 2015;83:809-19.
[48] Katayama Y, Lio S, Veerapun S, Uchiyama T. Investigation of Blade Angle of an Open Cross-Flow Runner. Int J Turbo Jet-Engines 2015;32.1:65-72.
[49] Costa Pereira NH, Borges JE. Prediction of the Cross-Flow Turbine Efficiency with Experimental Verification. J Hydraul Eng 2017;143.1:04016075.
[50] Ulrich KT, Eppinger SD. Product Design and Development. 5th int ed. New York: McGraw-Hill; 2012.
[51] Giesecke J, Mosonyi E. Wasserkraftanlagen: Planung, Bau und Betrieb. 5th ed. Heidelberg: Springer; 2009.
[52] Young DF, Munson BR, Okiishi TH, Huebsch WW. Introduction to Fluid Mechanics. 5th ed SI version. Hoboken: John Wiley & Sons; 2012.
[53] Ossberger GmbH + Co. Cross-Flow Turbine Excels at Power Plant Project in Santiago de Chile. Zek HYDRO April 2014;46-7.
[54] Ossberger GmbH + Co. Small Hydropower Plant in Chile with OSS-

BERGER Cross-Flow Turbines. Zek HYDRO April 2013;58-9.
[55] Klebsattel G, Schneider K, Wirth D. Bau einer Kleinwasserkraftanlage mit Durchstromturbine an der Wehratalsperre. Wasserwirtschaft 2000;90.4:192-7.
[56] Erdmannsdorfer H, Ossberger GmbH + Co. Small is Beautiful, http://www.ossberger.de/cms/fileadmin/_migrated/content_uploads/1-2-10_14.pdf; [accessed 12.10.16].
[57] Ossberger GmbH + Co. Grosse Dhunn-Talsperre - "Thermorussel" Speist Durchstrom-Zwillinge. Zek HYDRO December 2014;28-30.
[58] Ossberger GmbH + Co. Neues Kraftwerk an der Schleuse Leerstetten am Main-Donau-Kanal Geht in Betrieb. Zek HYDRO October 2013;62-4.
[59] AEIT-TAA Technisches Seminar, Ossberger GmbH + Co. Nutzung Kleiner Fallhohen mit Ossberger-Turbinen, http://www.aeit-taa.org/Documenti/AEIT-TAA-2014-05-08-Bolzano-Wirth-Ossberger.pdf; May 2014 [accessed 12.10.16].
[60] Ossberger GmbH + Co. Das Beste aus 40 Kraftwerken Konzentriert. Zek HYDRO June 2013;47-50.
[61] Ossberger GmbH + Co. Alte Betonzylindermauer in Modernes Durchstromkraftwerk Verwandelt. Zek HYDRO June 2014;26-8.
[62] Ossberger GmbH + Co. Video Water Power Station Cyimbili, http://www.ossberger.de/cms/en/hydro/the-ossberger-turbine-for-asynchronous-and-synchronous-water-plants/video-water-power-station-cyimbili/; [accessed 12.10.16].
[63] Gloss SP, Wahl JR. Mortality of Juvenile Salmonids Passing through Ossberger Cross-Flow Turbines at Small-Scale Hydroelectric Sites. Trans Am Fish Soc 1983;112.2A:194-200.
[64] Ossberger GmbH + Co. Neues Durchstrom-Duo Verdoppelt den Stromertrag. Zek HYDRO August 2012;46-8.
[65] Boni M. Schlossmuhle Frauenfeld in der Schweiz: Volle Wasserkraft voraus! Wasserkraft Energie 2013;4:2-10.
[66] Ossberger GmbH + Co. Ungleiches Paar im Wechselspiel. Zek Wasser August 2007;30-1.
[67] Ossberger GmbH + Co. Maschinenwechsel Macht Sich Bezahlt. Zek Wasserkraft August 2008;26-7.
[68] Ossberger GmbH + Co. Umweltfreundliche Stromerzeugung auf der Engstligenalp. Zek Wasserkraft October 2011;22-5.
[69] Ossberger GmbH + Co. Turbinenwechsel in der Geistermuhle. Zek HYDRO June 2012;54-5.
[70] Ossberger GmbH + Co. Die Sichere Losung Fur Einen Grenzfall. Zek Wasserkraft April 2011;21-3.
[71] ANSYS Inc. ANSYS CFX Modeling Guide. Cecil Township: ANSYS Inc.; 2015.
[72] ANSYS Inc. ANSYS CFX Reference Guide. Cecil Township: ANSYS Inc.; 2015.
[73] ANSYS Inc. ANSYS CFX Theory Guide. Cecil Township: ANSYS Inc.; 2015.
[74] NPARC Alliance CFD Verification and Validation Website. Overview of CFD Verification and Validation, https://www.grc.nasa.gov/WWW/wind/valid/tutorial/overview.html; [accessed 30.10.16].
[75] NPARC Alliance CFD Verification and Validation Website. Validation Assessment, https://www.grc.nasa.gov/WWW/wind/valid/tutorial/valassess.html; [accessed 30.10.16].
[76] Figliola RS, Beasley DE. Theory and Design for Mechanical Measurements. 5th ed. Hoboken: John Wiley & Sons; 2011.
[77] ANSYS Inc. ANSYS AIM Documentation. Cecil Township: ANSYS Inc.; 2017.